Journal of Physics: Energy

TOPICAL REVIEW

Metal oxide charge transport layers in perovskite solar cells—optimising low temperature processing and improving the interfaces towards low temperature processed, efficient and stable devices

Yantao Wang[1], Aleksandra B Djurišić[1,5], Wei Chen[1], Fangzhou Liu[1], Rui Cheng[2], Shien Ping Feng[2], Alan Man Ching Ng[3] and Zhubing He[4]

[1] Department of Physics, the University of Hong Kong, Pokfulam Road, Hong Kong, People's Republic of China
[2] Department of Mechanical Engineering, the University of Hong Kong, Pokfulam Road, Hong Kong, People's Republic of China
[3] Core Research Facilities, South University of Science and Technology, No. 1088, Xueyuan Rd., Nanshan, 518055 Shenzhen, People's Republic of China
[4] Department of Materials Science and Engineering, Shenzhen Key Laboratory of Full Spectral Solar Electricity Generation (FSSEG), Southern University of Science and Technology, No. 1088, Xueyuan Rd., Shenzhen 518055 Guangdong, People's Republic of China
[5] Author to whom any correspondence should be addressed.

E-mail: dalek@hku.hk

Keywords: metal oxide, perovskite solar cells, charge transport layers

OPEN ACCESS

RECEIVED
25 July 2020

REVISED
19 September 2020

ACCEPTED FOR PUBLICATION
3 November 2020

PUBLISHED
15 December 2020

Abstract

In this review, we will discuss recent progress in metal oxide charge transport layers in perovskite solar cells (PSCs). While a large number of PSCs have at least one metal oxide charge transport layer, here we focus on the progress towards the achievement of high efficiency devices with metal oxide layers prepared under mild deposition conditions, with the ultimate goal being the devices containing metal oxide layer both below and above the perovskite layer to achieve improved stability. Thus, we will provide an overview of recent progress in metal oxides deposited below the perovskite layer (electron transport layers in conventional architecture PSCs, hole transport layers in inverted architecture PSCs), followed by the progress in devices containing both top and bottom metal oxide charge transport layer, and briefly introducing other possible uses of metal oxides in PSCs. For these various applications of metal oxides, we will discuss different approaches (doping, surface treatments, interface modifications) commonly employed to improve device performances, and finally we will provide a brief overview of the characterisation techniques commonly employed to obtain insights into physical mechanisms responsible for the observed device performance. While for several of the experimental techniques extensive reviews exist, this is not the case for all the techniques, and the perovskite literature commonly lacks cautions in interpretation, guidelines on avoiding artefacts, and general overview of what techniques need to be employed for comprehensive device characterisation.

1. Introduction

Perovskite solar cells (PSCs) have been attracting considerable attention due to their rapidly increasing efficiency since the first report on a solid-state PSC in 2012. The certified record efficiency is currently exceeding 25%, as illustrated in figure 1, outperforming not only other emerging single-cell photovoltaics (PV), but also more established thin film photovoltaics technologies, such as thin film Si, CIGS and CdTe solar cells. The first reports of PSCs commonly involved a structure closely resembling a solid-state dye-sensitised solar cell (DSSC), with mesoporous TiO_2 on fluorine-doped tin oxide (FTO) glass electrode as an electron transport layer (ETL), and 2,2′,7,7′-tetrakis[N,N-di(4-methoxyphenyl)amino]-9,9′-spirobifluorene (spiro-OMeTAD) as a hole transport layer (HTL), which is classified as a mesoscopic conventional PSCs. Schematic diagrams of different types of PSCs, namely conventional vs. inverted, planar

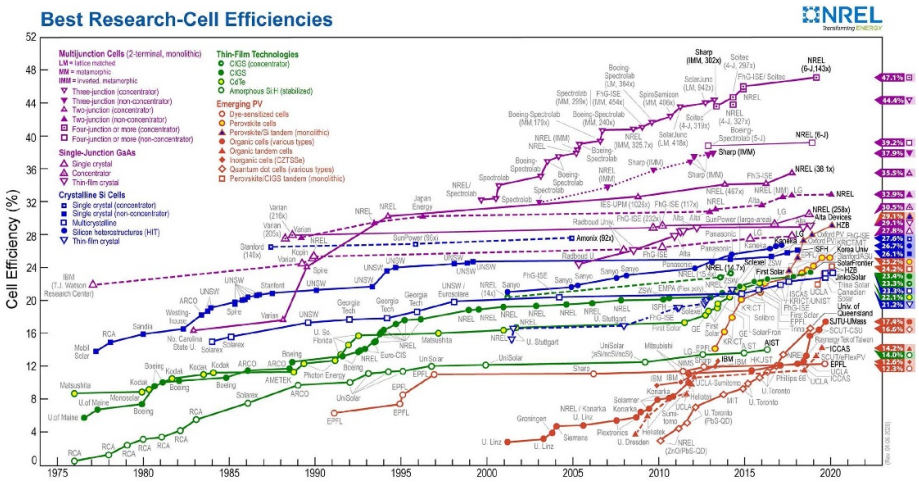

Figure 1. Efficiency chart of different solar cell technologies. This plot is courtesy of the National Renewable Energy Laboratory, Golden, CO, USA.

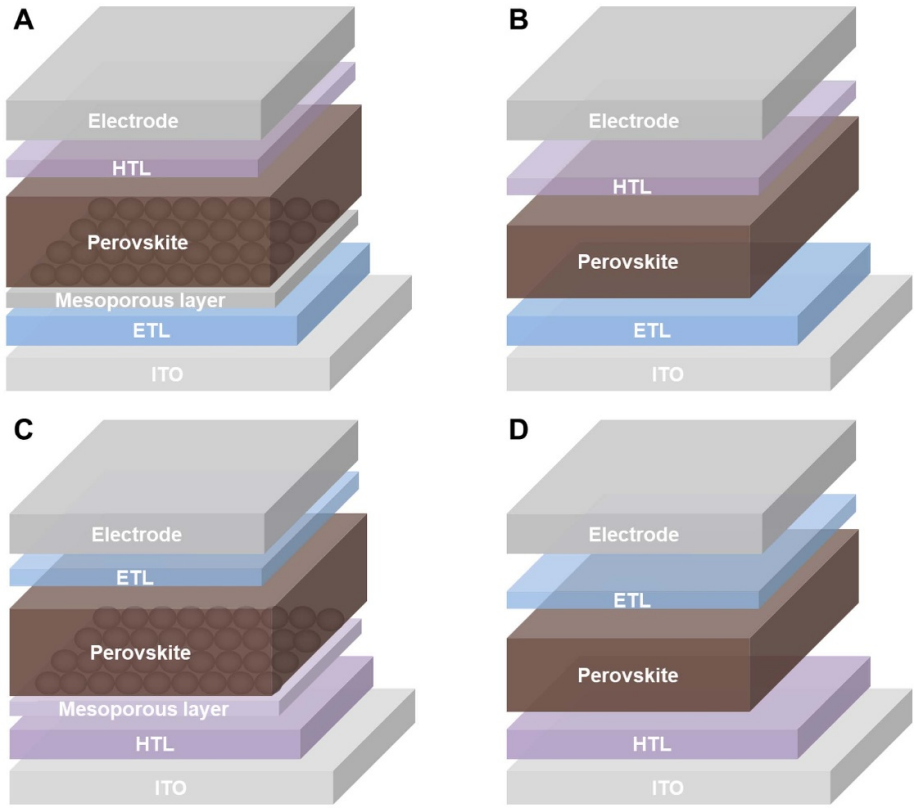

Figure 2. Schematic diagram of different types of perovskite solar cells. (a) Mesoscopic conventional PSC; (b) planar conventional PSC; (c) mesoscopic inverted PSC; and (d) planar inverted PSC.

vs. mesoscopic, are illustrated in figure 2. The majority of mesoscopic devices are using the conventional n-i-p architecture, although there have also been reports of the mesoscopic inverted device with p-i-n architecture [1, 2]. Mesoscopic architectures in general have an advantage in terms of efficiency and stability. However, planar devices which lack a mesoscopic layer can result in significant simplification of the device fabrication, and can allow a reduction in annealing temperature compared to mesoscopic devices since there is no need for removal of organic binders and improved crystallisation by high temperature annealing. While there have been reports on mesoscopic layers with low deposition temperature [3, 4], the majority of mesoscopic devices require high processing temperature. In contrast, there are more frequent reports of low temperature deposition for the planar oxide layer. In addition, reported efficiencies of planar devices have been rising, and there have been a number of reports of planar devices with efficiencies exceeding 20% in recent years [5]. For example, a planar device with efficiency of 23% has been recently reported, as illustrated

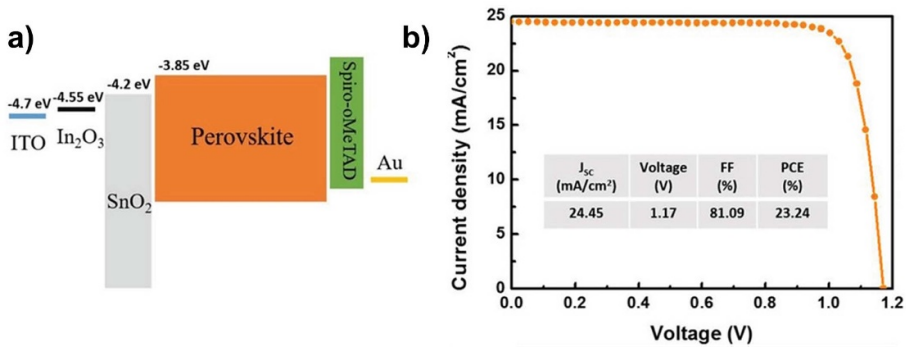

Figure 3. (a) Energy level diagram of PSCs based on In_2O_3/SnO_2; (b) The optimized device based on In_2O_3/SnO_2 ETL. Reproduced with permission from [6].

in figure 3 [6]. Overall, the highest achieved efficiencies to date are 23.32% for conventional [7] and inverted [8] planar PSCs. Thus, while the mesoscopic cells still retain a performance advantage, the performance gap between mesoscopic and planar devices has been narrowing in recent years, resulting in rising interest in planar devices and as a result the question of planar vs. mesoscopic architecture is not considered as settled [5]. In particular, planar architectures with low metal oxide processing temperature are of significant interest for flexible PSC applications. For recent reviews of flexible devices, see [9, 10].

For all the device architectures, a vast majority of PSCs will contain at least one metal oxide layer, and the main motivation in using metal oxides is to achieve improved stability compared to organic materials. While the maximum theoretical efficiency of the perovskite solar cells has not yet been reached, in recent years the research focus has been shifting from improving the efficiency to improving the stability of the devices, which remains a significant problem [5]. For a recent review of stability issues and degradation mechanisms in PSCs, see [11]. The majority of literature reports on cell stability involve demonstrations of shelf-life stability, i.e. devices stored in the dark in either ambient or inert environment. This results in exaggerated estimates of stability, since PSCs typically exhibit accelerated decay of performance when exposed to illumination (especially UV illumination), elevated temperature, and electrical bias. To standardise measurement conditions and enable faster progress towards being able to compare results from different research groups and thus draw more accurate conclusions on methods for improving device stability, International Summit on Organic Photovoltaic Stability (ISOS) protocols have been recently updated for PSCs [12]. In addition to the usual issues in characterising PSCs (taking care of hysteresis and scan rate dependence if any), the need for characterisation under bias and light-dark cycling has also been recognised [12]. With the wider adoption of these protocols, faster progress towards improving device stability is expected.

Increasing interest in improving the device stability has led to increasing interest in metal oxide charge transport layers, as well as the exploration of possibilities of both top and bottom oxide charge transport layer in an attempt to improve device ambient stability, since all-inorganic charge transport layers are expected to result in superior stability [5]. The stability advantage of metal oxide charge transport layers is typically pronounced when comparing them to moisture-sensitive organic materials, such as poly(3,4-ethylenedioxythiophene):poly(styrenesulfonic acid) (PEDOT:PSS) [13, 14], although there have also been demonstrations of improved performance compared to phenyl-C61-butyric acid methyl ester (PCBM)[15] and Spiro-OMeTAD [16]. In addition, organic materials which require dopants, such as Spiro-OMeTAD, may result in inferior stability at elevated temperatures or under illumination, i.e. conditions leading to dopant diffusion.

A good charge transport layer (CTL) should exhibit favorable energy level alignment with the perovskite for efficient charge extraction, have good charge mobility to allow efficient extraction, have low optical absorption, and it should also lead to low interfacial defects and consequently low recombination losses at interfaces [17–19]. Many different metal oxides can satisfy the first three conditions; for a detailed review, see [18]. In addition, they can be prepared using a variety of methods from inexpensive precursors, and many of those methods are compatible with low temperature processing (this is material dependent though, and some oxides are more likely to yield high quality films processed at low temperature compared to others) [18, 19]. For an overview of metal oxide synthesis methods, with the focus on oxide nanostructures, see [20]. Typically, the most problematic part in preparing a good CTL is the achievement of low interfacial defects and low recombination losses at interfaces. In addition, the perovskite crystal quality is significantly affected by the underlying CTL [13]. For example, the contact angle of the CTL for the perovskite solution affects the wetting of the surface and consequently the nucleation and growth of the perovskite film [13]. One useful

parameter to characterise the interface between different charge transport layers and the perovskite is surface recombination velocity, with lower surface recombination velocity (SRV) typically resulting in better performance [17]. Some of the common charge transport layers, such as TiO_2 and NiO_x, were found to have small values of SRV, consistent with efficient solar cells [17]. However, it should be noted that, depending on the deposition conditions, SRV for the same material can exhibit significant variation [17].

In general, the characterisation of the interfaces in the device is key to understanding the the correlations between the PSC performance and the CTL choices. We will therefore discuss various characterisation methods and what information can be extracted from them after summarising progress made for metal oxide charge transport layers in recent years. Thus, we aim to provide update on recent developments in the PSC field related to metal oxide charge transport layers to experienced perovskite researchers, while at the same time provide some information on various characterisation methods needed to comprehensively characterise the devices to researchers who have recently joined this exciting and rapidly developing field.

2. Metal oxides as electron transport layers

Different ETL materials, including metal oxides, have been reviewed recently [19]. The goal of our work here, instead of providing yet another comprehensive list of everything that has been done, is to provide a brief update of the progress, focusing on low temperature deposition of metal oxides in planar devices, and interface treatments/modifications leading to improved efficiency and stability of PSCs. In this section, we will primarily discuss metal oxides as ETLs in the conventional architecture, since their application in inverted devices would require different process limitations in order to avoid damage to the perovskite layer. Metal oxide layers for ETLs in conventional architecture can be deposited by different methods, such as atomic layer deposition (ALD), chemical bath deposition (CBD), spin-coating nanoparticles, doctor-blading, screen-printing, sol–gel, sputtering, e-beam deposition, etc. The film deposition can be followed by post-deposition treatments, such as sintering/annealing, oxygen plasma, UV ozone etc depending on the deposition method and precursors used. Depending on the highest processing temperature needed to obtain high quality oxide layer, the substrate can be either fluorine doped tin oxide (FTO)/glass for high processing temperatures, or indium tin oxide (ITO)/glass for lower processing temperatures due to increased resistance of ITO if annealed at high temperature [21]. ITO on flexible plastic substrates could only be used if the processing temperature is below 150^o C. Depending on the deposition method and post-deposition processing, additional treatment, such as UV ozone treatment, may be needed to remove residual organics and improve the wetting of the oxide layer [22]. The same maximum processing temperature limitations in substrate selection also apply to HTLs in inverted architecture devices.

2.1. Low temperature deposition methods for metal oxide ETLs

Due to the interest in developing flexible devices compatible with low cost roll-to-roll processing, considerable attention has been devoted to low temperature deposition methods for various oxide materials. To achieve smooth and uniform thin oxide films deposited under relatively mild conditions, ALD has attracted significant attention. The technique is commonly used for depositing ETLs in conventional architecture devices, such as TiO_2 and SnO_2 [23, 24]. The deposited layers are typically amorphous, uniform and pinhole free, but the device performance is strongly dependent on the deposition conditions for the oxide layer. The compact and uniform nature of the ALD deposited films enables them to be used to protect the metal electrode from corrosion in ITO-free devices [25]. In addition to ALD, solution-based techniques with optimised parameters could also be used to prepare the films at low temperature, although in this case the level of uniformity is often worse compared to ALD, but overall performance of the device could be better due to differences in energy level alignment across the interface, interfacial defects, and wetting properties. Vapor deposition techniques, such as sputtering, could also be compatible with low temperature processing and used for both rigid and flexible substrate, for example sputtered SnO_2 layers [26]. Another technique of significant interest is spin-coating pre-fabricated nanoparticles [27, 28]. To achieve high performance devices with ETLs prepared by spin-coating nanoparticles, it is necessary to achieve good dispersion of nanoparticles in the processing solvent (commercial dispersions are available for some of the materials). In addition, the number of spin-coating steps may need to be optimised and interface modifications may be needed to maximise the performance [27]. Alternatively, optimisation of post-deposition treatment can also result in significant performance improvements [28].

2.2. Common metal oxide materials

Different *n*-type oxide materials have been explored as ETLs to date. The initial reports of perovskite solar cells commonly employed TiO_2 as ETL, and TiO_2 still remains commonly used despite its drawbacks, such as high processing temperature. Although lower processing temperature and milder deposition conditions have

been achieved in some cases [9, 29], such studies remain scarce and most of the high efficiency devices still use TiO_2 processed at high temperature. Furthermore, the use of TiO_2 can result in decreased stability of the devices under UV illumination [30]. Although this can be improved by using various interfacial layers [30], there is significant interest in possible replacement of TiO_2 since in addition to discussed drawbacks it also commonly has relatively low electron mobility, which can even be lower than that of the perovskite itself [31].

ZnO and SnO_2 are alternative ETL oxide materials with higher electron mobilities, which can be prepared in good quality by low temperature deposition. While ZnO can be readily prepared by a variety of methods in a variety of nano structured morphologies [31], SnO_2 has superior chemical stability compared to ZnO [25]. Nevertheless, due to the ease of deposition, ZnO ETLs have been extensively investigated for application in PSCs. For details on this particular material, see a recent review [31]. Here, we will briefly discuss the important issues which limit the performance of PSCs with ZnO ETL, and discuss more promising TiO_2 alternatives, such as SnO_2, in more detail. Significant limiting factor for ZnO devices is the large surface recombination, attributed to large surface defect concentrations, which results in low fill factors and consequently lower efficiencies [31]. In addition, perovskite deposited on ZnO can decompose during annealing, which has been attributed to the deprotonation of methyl ammonium in contact with ZnO, facilitated by the chemisorbed species on the surface [31]. The deprotonation reaction leading to decomposition during annealing is dependent on the surface polarity of ZnO [32], and the surface polarity also affects photo generated carrier recombination in purely inorganic perovskite $CsPbBr_3$ [33]. However, ZnO could be potentially useful in all-inorganic $CsPbI_2Br$ perovskite solar cells, where improved performance was achieved with SnO_2/ZnO bilayer ETL compared to SnO_2 due to improved electron extraction [34, 35].

SnO_2 is generally considered as a suitable replacement for TiO_2 in planar devices since it can be deposited at relatively low temperatures and it can potentially exhibit negligible hysteresis in planar devices [22, 36]. In addition, solar cells with SnO_2 ETL exhibit improved stability under UV illumination compared to those with TiO_2 [22], since SnO_2 typically does not exhibit significant photocatalytic activity. Planar devices using SnO_2 on rigid substrates with efficiency $\geq$20% have been reported by a number of research groups [22, 27, 28, 36–51], while for flexible substrates over 18% has been reported [37, 52]. It should be noted that while negligible hysteresis has been demonstrated in devices with SnO_2 ETL [22, 37, 38, 41, 43, 51, 53], there have also been reports of SnO_2 based PSCs which exhibited significant hysteresis and/or performance dependence on scanning rate for different deposition methods, including ALD, CBD, spin-coated quantum dots, etc [22, 28, 36].

2.3. Approaches to improve performance of SnO_2 and ZnO ETLs

As mentioned, ZnO-based devices can suffer from performance impairment due to the instability of the perovskite/ZnO interface, while hysteresis, as well as interfacial recombination losses, can occur for both ZnO and SnO_2. Common approaches to deal with these problems include doping, interface modifications and device optimisation in general, as well as use of bi- or multilayer ETLs.

2.3.1. Doping

Doping has been more commonly used for SnO_2 compared to ZnO. Nevertheless, doping of ZnO has been attempted, and the common dopant used has been aluminium [54–56]. Aluminum doped ZnO (AZO) has been used in both inverted [54] and conventional [55] architectures. It was found to result in improved performance compared to ZnO [54], while it performed worse compared to SnO_2 and contributed to different degradation mechanisms in the perovskite [55]. It should be noted, however, that device degradation is a complex process with multiple contributing factors, and thus a comparison between two ETLs may produce different results for different perovskite composition or deposition method, or for different device architecture. In comparison, a greater variety of dopants has been used for SnO_2 doping. Possible dopants for SnO_2 reported in the literature include Zr [57], Ru [51], Sb [22, 50], Li, Mg, Y, and Nb [22]. Organic 'dopants', such as triphenylphosphine oxide and poly(vinyl pyrrolidone) have also been reported [58, 59].

2.3.2. Interface modification and device optimisation

The problem of instability of organic-inorganic perovskite in contact with ZnO can be mitigated by passivating surface defects, for example by doping [31], controlling the surface polarity (Zn- vs. O-terminated) [32], or by surface passivation, for example using alumina or organic materials [31], such as (2-aminothiazole-4-yl)acetic acid [60]. The use of monolayer graphene for passivating the ZnO surface to prevent perovskite decomposition has also been demonstrated, and high efficiency exceeding 21% (combined with the use of novel passivating material for perovskite) has been achieved [61]. In another

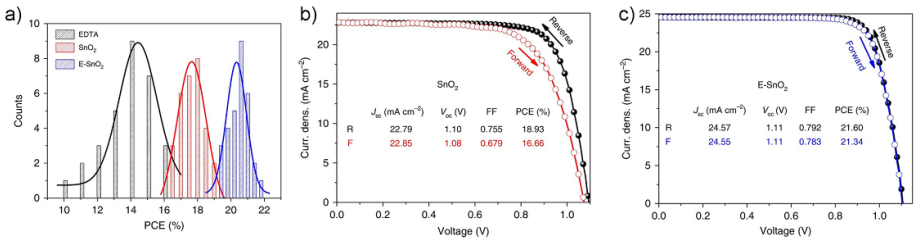

Figure 4. (a) The PCE distribution histogram of the planar-type PSCs based on different ETLs. The JV curves of the device with (b) SnO_2 and (c) E-SnO_2 measured under both reverse- and forward-scan directions. Reproduced with permission from [37].

example of high efficiency (≥21%) ZnO-based PSCs, the ZnO surface has been passivated by a thin layer of MgO and protonated ethanolamine [62].

Different from interface instability observed for ZnO, recombination losses and hysteresis are generally more complex phenomena. Since hysteresis is mainly attributed to charge accumulation, it could be addressed by adjusting the energy level alignment at interfaces and reducing interfacial defects. Thus, the hysteresis could be reduced by using interface modifications, or adjusting the composition of the perovskite layer, for example adding Rb [36], which was found to reduce hysteresis both for ALD and CBD-deposited SnO_2. However, the most common approach to increase the efficiency, reduce hysteresis, and further improve the stability of SnO_2-based PSCs remains interface modification, either by adjustment of preparation conditions or by surface modifications. For example, in ALD devices, the interface dipole at SnO_2/perovskite interface and consequently the electron extraction barrier and the device hysteresis was found to be dependent on the source of oxygen used (water, oxygen plasma, ozone) during the ALD growth [25]. The largest hysteresis was observed with when water is used as oxidant, and it also resulted in the formation of a gap state which worsened the hole blocking capability of SnO_2 [25]. Self-passivation by the precursor was also reported to be beneficial for the performance of devices with ALD-grown SnO_2 [46]. The hole blocking can also be negatively affected by SnO_2 morphology if a deposition method different from ALD is used, and this can be improved by using a thin insulating layer, such as MgO, between SnO_2 ETL and the FTO or ITO electrode [63]. In addition to improved electron collection and hole blocking, the surface treatments typically improve the performance of devices with SnO_2 ETL, as well as other oxide ETLs, by reducing interfacial traps and improving the crystallisation of the perovskite (this also applies to the use of bilayer structures).

Common surface treatments used to improve wettability of perovskite solution, such as UV-ozone, can also have beneficial effect on overall device performance and a decrease in recombination [53], but they may not be sufficient to guarantee good performance depending on the starting conditions of the SnO_2 surface determined by its preparation method and conditions, and thus different surface treatment molecules may be needed to further improve the performance. Examples of different surface treatment molecules and/or interfacial layers include $TiCl_4$ [22], TiO_2/SnO_2 bilayer [22, 39], fullerene-based molecules/SnO_2 bilayers [22, 38, 44, 64], EDTA [37], KCl [40, 52, 65, 66], KNO_3 [66], $SnCl_2$ [67], amino-functionalized polymer [68], nitrogen-doped graphene oxide [69], chemically modified graphene [49], SnO_2/CdS [70], imidazolo acetic acid hydrochloride [41], ammonium chloride [43], acetic acid [45], carbon dots [71], PFN-Br [72], fluorinated ionic liquid [48], diethylenetriaminepentaacetic acid [27], etc. Obviously, different types of interface modifiers can result in improvements of device performance. Nevertheless, the use of alkali chlorides [40, 52, 65, 66], the use of molecules capable of interaction with the oxide on one end and perovskite on the other end [41], and the use of molecules containing ammonium group [43] seem to be applicable to more than one type of metal oxide CTL and are likely to result in significant improvements of the device performance.

Such improvements typically reduce interfacial defects and consequently reduce recombination losses, improve the efficiency as well as stability of the devices, and can also reduce the hysteresis. For example, the hysteresis in devices with EDTA-SnO_2 has been dramatically reduced, as shown in figure 4, which has been attributed to a significant reduction in defect density, which in addition to the reduction of hysteresis facilitates the achievement of high efficiency for both rigid and flexible devices [37]. This approach, namely low temperature deposition of SnO_2, combined with its surface modification, has been demonstrated to be effective for obtaining flexible devices with efficiency exceeding 18% for multiple approaches (different deposition details, different surface modifying agents) [37, 52]. Similarly, fullerene-derivative modification of SnO_2 also resulted in significant improvement in efficiency, stability, and the reduction in hysteresis, attributed to not only in enhanced electron extraction by modifying energy level alignment, but also in improved orientational order of the perovskite film deposited on top of the ETL [38]. The reduction of

recombination losses and the reduction of hysteresis associated with interfacial layer-induced improved interface quality can result not only in improved efficiency, but also in improved stability [38, 41], confirming that interfaces have a critical role in PSC performance. Thus, interfacial modifications and/or the use of multilayer CTLs can potentially reduce charge accumulation at interface and consequently improve not only efficiency but also the stability of the devices [50].

2.3.3. Multilayer and composite ETLs

In general, bilayer or multilayer ETLs can be used to improve the device performance, and various multilayer ETLs containing ZnO, as well as other ETL material combinations have been reported, such as PCBM/Mg:ZnO [73], ALD-TiO_2/SnO_2/PCBM [29], HI-modified TiO_2/SnO_2 [74], ALD-TiO_2/SnO_2 [75], In_2O_3 /SnO_2 [6], PCBM/AZO/triphenyl-phosphine oxide [56], etc.

In addition to bilayers or multilayers of different materials, it is also possible to achieve performance improvement using bilayers based on the same material. For example, various bilayer SnO_2/SnO_2 structures have also been reported, for example Sb:SnO_2/SnO_2, where improved performance was attributed to improved energy level alignment [50] Since the tin oxide properties exhibit strong dependence on the synthesis/deposition/post-deposition treatment conditions, combining the SnO_2 based layers with different preparation conditions enables adjustment in energy level alignment across the interface and consequently efficient charge extraction. In addition, improved performance and reduced hysteresis has been achieved by dual-coating of SnO_2 with different annealing temperatures compared to single coating, demonstrating strong dependence of performance on SnO_2 preparation [47]. Similar effect could be achieved by surface/interface modifications, and using multilayer ETLs consisting of other materials in combination with tin oxide. Finally, other approaches such as composite layers have been reported, including red carbon quantum dot-SnO_2 composite [76], carbon nanotube-SnO_2 composite [77], and a composite consisting of SnO_2 nanoparticles prepared by different methods [42].

2.4. Other oxide ETLs

In addition to these three commonly studied metal oxide materials (TiO_2, ZnO, and SnO_2), other n-type metal oxides have also been reported, such as $Zn_2Ti_3O_8$ [78], $BaSnO_3$ [79], α-Fe_2O_3/PCBM [80], WO_x [81], etc. For a recent review of ternary oxides as charge transport layers, both ETL and HTL, see [82]. However, these materials have not been extensively adopted, and while in individual studies these materials exhibit improved performance over more conventional material choices, they do not necessarily show clear advantages when considering the best performance devices obtained for SnO_2 or TiO_2. Furthermore, while in some cases advantages such as low processing temperature or the lack of significant hysteresis are clearly demonstrated, the obtained efficiencies are commonly below 20%. An exception would be WO_x, which was shown to result in high efficiency [81], although this material is not commonly used as an ETL. It should be noted, however, that these less commonly used materials have not been fully explored in particular when it comes to interface optimisation, and thus it is possible that some of them may offer improved performance in the future. Materials exhibiting no photocatalytic activity and resulting in devices with no hysteresis are of particular interest for further development.

3. Metal oxides as hole transport layers

Organic HTLs, such as PEDOT:PSS, Spiro-OMeTAD or poly(triaryl amine) (PTAA, or poly[bis(4-phenyl)(2,4,6-trimethylphenyl)amine) were widely used in perovskite solar cells and generated many high efficiency devices. However, their ambient and thermal stability, as well as in some cases the use of hygroscopic dopants, limit the long term stability of PSCs. Metal oxides or other inorganic materials have intrinsically better thermal stability and charge conductivity, and have been widely used as charge transport layers.

3.1. NiO_x hole transport layers

One of the most commonly used metal oxide HTLs is nickel oxide, NiO_x, which exhibits p-type conductivity without intentional doping, attributed to nickel vacancies. Unlike conventional architecture devices with metal oxide ETL, inverted devices with NiO_x HTL commonly do not exhibit significant hysteresis, i.e. while in conventional devices the observation of hysteresis is more common than no hysteresis, opposite trend is observed for inverted devices. However, it should be noted that hysteresis in NiO_x-based devices, in particular after ageing, can sometimes be observed, and non-capacitive dark hysteresis in NiO_x-based devices has been studied [83]. The observation of hysteresis was attributed to the electrochemical reactions at the interface under bias and/or ionic migration, and the effect was mitigated by an interfacial layer [83].

3.1.1. The deposition of NiO_x

Similar to other commonly used metal oxides, NiO_x can be deposited by a variety of methods, including flame-assisted chemical vapour deposition [84], spray combustion method [85], controlled oxidation of Ni [86], anodic electrodeposition [87], chemical bath deposition [88], spin-coating of nanoparticles [14, 89], sputtering [90], sol–gel deposition [91], combustion synthesis [91], etc As with all metal oxides, the properties of prepared NiO_x films are dependent on the deposition method, deposition conditions, and post-deposition processing, since these factors affect the resulting concentration of nickel vacancies, which are primarily responsible for the p-type conductivity of NiO_x. In addition, the surface properties of NiO_x affect the properties of the perovskite grown on top, and differences in the interfacial defects, charge collection, and charge recombination can result in significant differences in device performance, as evident from comparison of different deposition methods performed by the same research group (so that variability in perovskite layer deposition would not apply), where not only differences in the efficiency but also stability were observed [91]. There are numerous factors which can affect the properties of the resulting NiO_x layer, such as precursors and solvents used, solution concentration, etc In addition to those common and obvious factors, others such as precursor solution ageing time [92], also need to be taken into account when preparing reproducible devices. Among post-deposition processing, annealing is commonly used, and different annealing protocols have been investigated in the literature [93]. In general, the results of post-deposition processing will depend on the starting properties of NiO_x, and the same annealing protocol for example is unlikely to give the best results for film prepared by different methods. Furthermore, the effect of post-deposition treatments, such as annealing, oxygen plasma, and/or UV ozone have significant effect on the properties of NiO_x. For example, solution processed NiO_x can contain nickel hydroxide phases, which get converted to NiOOH upon exposure to oxygen plasma and annealing [94].

Among different deposition methods, spin-coating pre-fabricated nanoparticles is of particular interest due to its compatibility with flexible plastic substrates [14, 89]. Nanoparticles could also be synthesized by different methods, including micro plasma synthesis [95], and chemical precipitation method [14]. Microplasma synthesis has an advantage of obtaining ultrasmall nanoparticles [95], but the obtained device efficiency was quite low for this fabrication method. Due to multiple factors affecting the final efficiency (device architecture, perovskite quality, etc) and insufficient characterisation, it is not fully clear whether the poor performance was due to NiO_x or other factors, similar to other works reporting low efficiency cells with NiO_x HTL [92]. In general, synthesis method and growth conditions for the nanoparticles will affect not only their physical size, but also their dispersability in different solvents, which is affected by the surface properties of nanoparticles and which ultimately affects the film quality for films prepared by spin-coating the nanoparticles. While both undoped and doped nanoparticles can be prepared, it should also be noted that the introduction of the dopant can affect the dispersability of the doped nanoparticles due to the changes in surface properties (surface defect concentrations), and thus care needs to be taken in optimising the synthesis when dopants are introduced. For a detailed review on reactivity and stability of nanoparticles, including surface microenvironment and dispersion stability, see [96].

3.1.2. Doping of NiO_x

Different dopants have been proposed for NiO_x, such as Zn [97], Li [13, 98], Cs [99], Cu [14, 89, 100], Mg [90], etc. Co-doping with different elements, such Li-Cu and Li-Mg, is also possible [101]. For a detailed review of doped NiO_x in inverted PSCs, see [101]. In some cases, where divalent dopant, such as Zn [97], is used to replace Ni^{2+} it is not fully clear what would be an advantage of such a dopant, since the only way that dopant could contribute charge carriers is by generating additional defects in the crystal lattice, which would inevitably reduce the charge mobility. While the theoretical calculations have shown that the introduction of Zn is favourable for the formation of nickel vacancies [97], when considering the dopant choice one needs to carefully consider the effects of dopant. The situation is also more complex when the dopant has multiple valence states, such as for example Cu which can be introduced as Cu^{+} or Cu^{2+} [89]. While the conductivity is directly proportional both to charge carrier concentration and mobility, the effect of those parameters on photovoltaic performance is more complex. Generally, higher carrier mobility means faster charge collection at the electrode and lower charge accumulation and lower recombination losses, but other parameters, such as energy level alignment across the interface are more likely to have more significant effect on the charge carrier collection efficiency. For example, in Mg-doped NiO_x observed increase in conductivity was small, while there was a significant shift in the work function, resulting in improved charge collection [90].

3.1.3. Organic dopants and surface/interface modifications

In addition to conventional inorganic dopants, similar to SnO_2, organic doping with different organic molecules (acceptor molecules with high electron affinity in this case) has been reported for NiO_x [102, 103]. This approach typically results in the shift in the energy levels of NiO_x ensuring improved charge collection

[102, 103], and increased conductivity of NiO_x [103]. Since the approach involves the deposition of organic molecule on the surface, the quality of the perovskite layer grown on top is typically improved as a result, similar to surface treatments and/or deposition of interfacial layers. The reported surface modifications of NiO_x include various organic materials, such as PTAA [104], ferrocenecarboxylic acid [105], cysteine [100], diethanolamine [106], as well as inorganic materials, such as alkali chlorides [107, 108], and hybrid organic-inorganic materials, such as Mg-organic interlayer [83]. The use of optimised synthesis, doping and/or interfacial modifications in NiO_x-based inverted devices has resulted in a number of reports of devices with efficiency exceeding 20% [91, 102, 103], with the highest efficiency reaching 22.1% [102] for rigid and 20.0% for flexible devices, which is a significant achievement considering that the performance of inverted PSCs generally lags behind that of conventional ones.

3.2.Other oxide HTLs

Along with commonly investigated NiO_x, other metal oxides have also been investigated for applications as HTLs, but similar to ETLs less commonly reported choices typically result in lower efficiencies compared to the best reported results for the commonly used materials. Other oxide HTLs listed in the literature include TiO_2-IrO_x alloy [109], indium doped $CuCrO_2$ [110], $ZnCo_2O_4$ and $NiCo_2O_4$ [111–113], WO_3-water-free PEDOT:PSS composite [114], Co_3O_4 [115], Cu_2O [116], etc. Unlike NiO_x, these materials typically result in devices with efficiencies below 20%, but the influence of the surface treatments and/or interface modifications for these materials has not been as comprehensively explored as in the case of NiO_x.

4. Devices with metal oxides as both ETL and HTL

Due to expected improvement in device stability, there has been considerable interest in the development of devices which use inorganic materials, most commonly metal oxides, as both top and bottom CTLs [5]. While this type of devices has been successfully achieved for all commonly used metal oxides, namely TiO_2, SnO_2, ZnO, NiO_x, as well as less commonly used Cu_2O [15, 16, 95, 116–118], and the stability was commonly improved [95, 116], the efficiency of the devices was quite low in some reported cases [95], while in others high efficiency devices have been demonstrated [15, 16, 116, 118]. Overall, the number of papers exploring this type of strategy has been small, primarily due to processing difficulties of depositing the top oxide layer without damaging the perovskite layer underneath, and reducing the density of traps at perovskite/top CTL interface to ensure good performance. For this reason, interlayers (commonly organic) are sometimes needed either between the perovskite and top CTL or between the top CTL and electrode.

4.1. Solution-processed CTLs

A main challenge to obtain metal oxide charge transport layer based device is the possibility of perovskite film being damaged by solvent for solution-processed metal oxide, as well as imperfect coverage of the top CTL film. To solve this problem, three approaches have been tried: (I) solvent engineering, which aims to disperse target metal oxide nanoparticles with proper solvents which would not significantly affect the quality of perovskite films [117, 119–121], assisted with mechanical dispersion when needed [118, 120, 122]; (II) interface engineering, which applies to either surface modification to nanoparticles [15, 116, 123, 124] or using bilayer CTL to passivate surface defects as well as enhance conductivity of corresponding charge transport layer [16, 118, 119]; (III) non-solution processing [125–127].

Different solvents in solvent engineering approaches have been reported to date. A possible approach to avoid damage to the perovskite layer is to use a commonly used anti-solvent such as chlorobenzene to disperse metal oxide nanoparticles [117]. This approach resulted in ITO/NiO_x/$MAPbI_3$/ZnO/Al devices with a maximum efficiency of 16.1% and significantly improved stability [117]. The ZnO ETL based device retained 90% of initial PCE after 60 days ageing in ambient, while the control device (PCBM as ETL) completely degraded after 5 days [117]. Other solvents used include isopropanol (IPA) used for dispersing indium doped ZnO (IZO) nanoparticles [120], 1-butanol [119], and mixed solvent (n-butanol: methanol: chloroform) [121].

To improve the dispersion of the nanoparticles, different surface modifications have been reported, such as stearate ligand [123], hexanoic acid [124], oleic acid [16], and C_{60}-Substituted Catechol (Fa) [15]. The Fa-ZnO-based PSCs reached efficiency of 19.34%, which was further increased to 21.11% by using Fa-ZnO dilute solution as anti-solvent. In addition to high efficiency, excellent stability was achieved, with t80 of 1600 h under 65° C continuous heating in ~ 30–50% RH ambient without encapsulation. The stability of devices with a dual oxide CTL (Cu:NiO_x as HTL and Fa-ZnO as ETL) was significantly enhanced compared to devices with PCBM ETL [15].

In this last example of nanoparticle surface modification, it can be observed that another ETL material, namely fullerene, was used. It is thus not surprising that bilayer CTL approaches have also shown to be

capable of yielding high efficiency devices. NiO_x bilayer with CuSCN and Spiro-OMeTAD was reported to yield maximum efficiencies of 14.4% and 16.3%, respectively [119]. However, device stability was the was the highest for NiO_x alone, followed by NiO_x/CuSCN and NiO_x/Spiro-OMeTAD based devices, which retained about 102%, 98%, 92% of their initial efficiencies, respectively, after 4 months ageing in ambient [119]. It should be noted that achievable efficiencies for the same HTL can be highly dependent on the processing conditions. For example, when CuSCN was spun on wet NiO_x surface, 19.24% efficiency and appreciable stability were achieved, with 95% of initial PCE retained after 1000 h at 60 °C continuous heating [118]. These devices exhibit improved thermal stability in air compared to single layer HTL devices, including those with commonly used Spiro-OMeTAD, which is generally known to have poor thermal stability [118]. Nevertheless, the use of Spiro-OMeTAD as a part of a bilayer HTL can result in quite respectable stability at RT. For example, combining the use of stable bottom ETL (SnO_2) and a top bilayer HTL (NiO_x with oleic acid/Spiro-OMeTAD) has resulted in high performance device with efficiency of 21.66% and negligible hysteresis, which maintained 90% of initial efficiency after 1200 h, exhibiting a significant improvement compared to devices containing only Spiro-OMeTAD [16].

4.2. Vapour-deposited CTLs

Compared to solution-based processing (including bilayer CTLs), vapour deposition approaches such as sputtering [125] achieved inferior performance which needs further optimization. In addition to sputtering, ALD approach to deposit oxide layers on top of the perovskite has also been investigated [126, 127]. It was found that the metal precursor could damage the perovskite layer, and that prevented the deposition of ZnO films by ALD on top of the perovskite, while SnO_2 could be deposited, but low efficiency and significant hysteresis were obtained [126]. Deposition of TiO_2 on top of PCBM to form a bilayer ETL was accomplished, resulting in the efficiency of 18.3%, with 97% of initial performance retained after storage in ambient for 1000 h [127]. In addition, devices with metal oxide CTLs on both sides could also be prepared by lamination, but in this case as well overall efficiencies could be low, in particular when transparent conductive oxide (TCO) electrodes are used on both sides [128]. Overall, the achievement of high efficiency devices with metal oxide layers used for both ETL and HTL is challenging, and the number of reports on PCE exceeding 20% has been scarce [15, 16]. The achievement of high efficiencies in devices using metal oxide CTLs on both sides of the perovskite layer likely requires the use of bilayer structures, and careful optimisation of interfaces and overall processing methods.

5. Other applications of metal oxides

In addition to their use as charge transport layers, metal oxides are also commonly used as interface or barrier layers. For this type of application, especially for barrier layers, ALD is a common deposition technique. ALD can form compact layers which would provide excellent protection against moisture penetration if the damage to the perovskite layer could be avoided. Generally, the use of water as an oxidant for ALD can result in the damage to the perovskite layer [126]. Nevertheless, the use of ALD for the deposition of barrier layers such as Al_2O_3 using water has been reported for a custom-built reactor [129]. A stacked Al_2O_3 encapsulation was shown to be sufficiently protective to not only ensure no significant degradation upon storage in ambient, but also to protect the devices from water immersion for 2 h [127].

Metal oxide layers are also commonly used as interfacial layers at the electrode, to adjust the work function of the electrode, and/or improve electrode stability. The commonly used oxide is MoO_x, in combination with Au or Al electrodes. However, it was recently reported that tantalum doped tungsten oxide Ta:WO_x exhibits superior performance, resulting in high stability perovskite solar cells [130].

In addition, highly doped metal oxides (conductive metal oxides) are commonly used as recombination layers in tandem solar cells. The problems which need to be resolved in the deposition of the recombination layer depends on what materials are used in the bottom cell. Typically, Si/perovskite and CIGS/ perovskite tandems could withstand harsher recombination layer deposition conditions, but there could still be problems with the deposition of a TCO contact on top of the perovskite cell. On the other hand, OPV/perovskite and all-perovskite tandems would require mild deposition conditions for the recombination layer, and it is desirable that the recombination layer would provide a good barrier to the processing solvents for the top perovskite cell [131]. It was found that while low temperature ALD could be used to grow AZO recombination layer on top of C_{60}, non-reactive nature of fullerene resulted in inferior nucleation of the AZO layer and consequently its poor barrier properties [131]. It was found that poly(ethylenimine)ethoxylated (PEIE) nucleation layer could significantly improve the quality of the AZO layer and its barrier properties against dimethylformamide, as well as significantly reduce its water vapour transmission ratio (WVTR) [131].

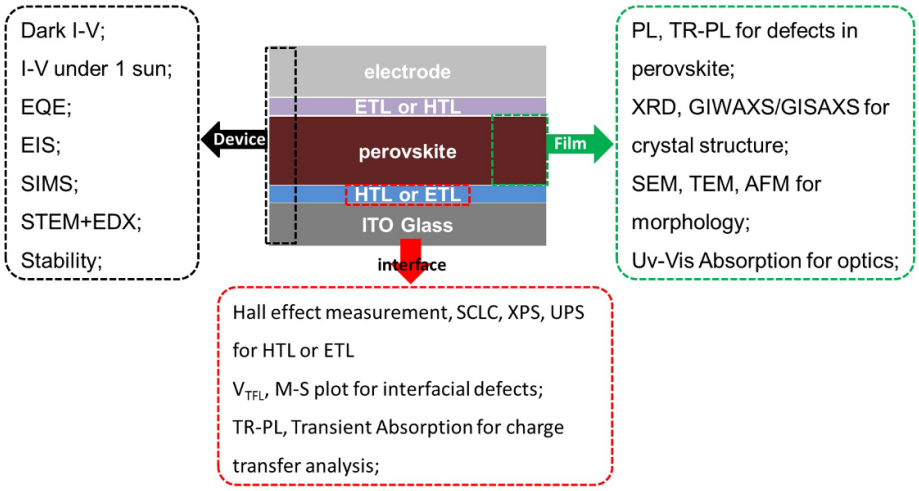

Figure 5. Schematic diagram of a PSC and relevant characterisation techniques applicable to different parts or the whole device.

Finally, various metal oxide-based composites have been investigated for PSC applications. For example, metal oxides have been incorporated into ambient-processed perovskite films to form a perovskite-metal oxide composite which resulted in high performance devices with significant stability enhancement [132, 133]. The use of perovskite metal-oxide composites in 'minimalist' CTL-free devices has also been reported [134]. Embedding NiO nanoparticles into the surface of perovskite layer prior to deposition of multi wall carbon nanotube electrodes for the enhancement of device performance has also been reported [135]. More complex devices containing various composites, such as substrate/NiO-perovskite/Al_2O_3-perovskite/SnO_2 coated carbon nanotube-perovskite, have also been reported [136]. Metal-oxide carbon composites, such as NiO_x-carbon spheres, have also been used as electrodes in PSCs [137].

6. Necessary characterisation techniques for understanding the effect of oxide layer on PSC performance

Different characterisation techniques common in literature on PSCs are shown in figure 5. For an overview of characterisation of metal oxides specifically, rather than entire PSC device, see [20]. Before we proceed with describing additional characterisation techniques which distinguish significant advances in understanding why certain material or interface modification works well from simple reports on possible approaches which can improve device performance, we will briefly mention what are the true basic characterisations which need to be done as a routine but necessary characterisation. Any manuscript on a solar cell must contain an evaluation of the solar cell performance, namely the measurement of *I–V* curves under one Sun simulated solar illumination. Dark *I–V* curve measurement should also be performed to check for any abnormalities in the *I–V* curve shape, even though these data are less commonly reported. The measurement details for *I–V* curves under illumination should be clearly specified, and sufficient characterisation provided, including light source used, scan rate, *I–V* curves for both forward and reverse scans, and *I–V* curves for different scanning rate. The inclusion of external quantum efficiency (EQE) measurements, with the cross-check of estimated short circuit current density, is highly desirable. Stability should also be evaluated, preferably using standardised ISOS protocols, which have recently been updated for PSC characterisation [12]. While a large number of papers report the stability on storage in ambient without illumination, truly relevant data on stability must include additional stresses (thermal stress, illumination) to make a valid claim that observed environmental stability improvement with dark storage is potentially practically relevant.

Next, x-ray diffraction (XRD) should be performed, to confirm the crystal structure of the perovskite and, if relevant, CTLs used. If new materials are introduced, it is highly advisable to collaborate with a crystallographer rather than simply try to identify the lines by comparison with databases and published literature, since this can lead to errors in identification of new structures, especially when lower-dimensional perovskites are introduced as capping layers. Finally, the energy level alignments across the CTL/perovskite interface are highly relevant for charge collection. Hence, ultraviolet photoelectron spectroscopy (UPS) is used to determine the work function of the CTL deposited by a certain method or treated with a certain surface treatment, and compared to a control sample to evaluate the effect of deposition conditions or surface treatments/interfacial layers on charge collection. The trends observed in UPS can then be further

verified by Kelvin probe force microscopy (KPFM), [43] which is one of the scanning probe microscopy modes available in any standard scanning probe microscope.

Finally, the evaluation of film quality is also a part of standard characterisation. Contact angle measurements to examine the wetting and spreading of the perovskite solution can also be a part of investigating the film quality. To examine the film quality, scanning electron microscopy (SEM) and atomic force microscopy (AFM) are the most basic techniques to characterise the morphology of the metal oxide film, as well as the morphology of the perovskite grown on the metal oxide. Defects such as pinholes, and obvious macroscopic differences, such as different grain sizes, can readily be discerned using these techniques. Unfortunately, these techniques do not provide information about smaller scale differences, such as point defect concentrations etc, which significantly affect the device performance. Here we will provide a brief discussion of relevant characterisation which are needed to fully understand the phenomena at perovskite/charge transport layer interfaces. Typically, a combination of optical, electrical and structural characterisation is critical to fully understand all the relevant processes contributing to the overall device performance. We will describe below the common techniques used, what kind of information they can provide, and if relevant what kind of experimental artefacts or issues with data interpretation can occur and how to avoid them. The experimental characterisation is often complemented with density functional theory (DFT) and/or molecular dynamics (MD) calculations, but the overview of those simulations is beyond the scope of this perspective, which primarily focuses on experimental work.

6.1. Structural and compositional characterisation

Grazing-incidence wide-angle x-ray scattering (GIWAXS) and grazing-incidence small-angle x-ray scattering (GISAXS) are scattering techniques commonly used for characterising the crystal structure of the perovskite layers, and they are also useful for characterisation of different layers in the device, in particular for the layers which have small thickness and/or do not have high degree of crystallinity. Since the incident angle of the x-ray is very small, diffractions of a thin films in GIWAXS is highly surface sensitive and the detected signals are much stronger than the XRD pattern measured for thin films in a conventional XRD instrument. Thus, more detailed lattice parameters of perovskite crystals and crystal orientation of the three dimensional and quasi-two dimensional perovskites can be obtained from GIWAXS. Furthermore, the use of two-dimensional detector and the varying angle of incidence can allow probing the structure at surface, bulk, and interface [20]. The information about material observed can be determined from characteristic q values, the integrated intensity of 2D GIWAXS pattern can be used for XRD pattern matching [138], and the degree of ordering is obtained from the resulting two-dimensional plots, where the observation of rings indicates the lack of ordering, spots indicate high degree of order [20], and arcs indicate an intermediate situation between ordered and disordered samples in terms of preferential orientation. In perovskite solar cells, GIWAXS has been used for identifying the crystallinity change after surface [139, 140] or sublayer [141] modification, as well as *in situ* crystallization monitoring during perovskite spin-coating [142].

X-ray photoelectron spectroscopy (XPS) is a surface-sensitive quantitative spectroscopic technique that measures the elemental composition, empirical formula, and chemical/electronic state of the elements that exist on the surface of a material. For instance, XPS technique was employed to analyze the content of dopants, and the ratio variation of N^{3+} and Ni^{2+} in the pristine and Cs and Cu doped NiO_x HTLs [89, 99]. The possible mechanism of increase of hole conductivity by doping of NiO_x could be supported by the XPS analysis. However, one needs to be careful in interpreting the data from XPS, in particular attempting to quantify oxygen deficiency in oxide layers, due to the difficulties in obtaining unique fit if just a broad peak or a peak and a shoulder are observed instead of distinct multiple peaks and consequent large uncertainties in the ratios of peak areas. Furthermore, it is difficult to quantify the ratios of dopants in different oxidation states if the resulting signal has low intensity, which can occur for dopants present at low concentrations [89].

Time-of-flight secondary ion mass spectrometry (ToF-SIMS) is an advanced technique that can simultaneously capture the full information of chemical distribution across a entire perovskite based device. It is one of the few techniques that can provide lateral and depth information of all components of PSC devices, which allows deep insight to cation distribution within the absorber layer and at interfaces and how they relate to device performance and stability [143, 144]. Depending on the instrument capability, ToF-SIMS enables 1D depth profiling, 2D lateral imaging, and 3D tomography, with a depth resolution of less than 1 nm and a lateral spatial resolution of less than 100 nm. Because useful information in the perovskite films (including grains, grain boundaries, surface, etc), different interfaces in the device, charge transport layers, and electrodes can be analyzed by ToF-SIMS through monitoring the chemical distributions. ToF-SIMS is very powerful tool for characterizing the perovskite materials and the corresponding devices. A detailed review of the role of ToF-SIMS in perovskite research can be found in [145]. However, despite the overall usefulness of the technique, in particular in studying the degradation mechanisms by comparing fresh and aged devices, artefacts are possible and care needs to be taken in interpreting the results. For

example, it was demonstrated that the A-site cation gradient is actually a measurement artefact caused by primary bismuth ion beam damage which leads to less secondary ion signals, and a new method was proposed to replace bismuth with cesium [146]. In addition, measurement instructions for avoiding artefacts have been provided [143]. Since ToF-SIMS instruments are often operated by dedicated technicians rather than researchers themselves, which provides limited flexibility in implementing modified instead of standard measurement protocols, at a minimum it is necessary to ensure that some control samples are included and tested on the same day to be able to identify artefacts if such occur.

Cross section energy dispersive x-ray spectroscopy (EDX) mapping can also provide element distribution of PSC devices, and it should be preferably used together with TOF-SIMS to provide accurate information on the location of elements in the device [107], as well as changes in the device composition as a result of ageing during stability testing. EDX is a common technique present in electron microscopes, both for SEM as well as transmission electron microscopy (TEM) instruments. Due to their higher resolution, TEM-based techniques, such as HR-TEM, STEM (HAADF mode) and EDX (or EELS) analysis are commonly used for for investigating the more detailed structure and elemental information in the perovskite solar cells (highly resolved device lateral morphology, charge transport/perovskite/electrodes interfaces). Moreover, the possible degradation mechanism of perovskite solar cells can be investigated by *in-situ* TEM. However, this technique require special sample preparation due to high sensitivity of perovskite materials to the electron beam exposure. More details regarding the application of TEM in perovskite solar cells can be found in the recent review papers [147, 148]. In addition, it should be noted though that EDX mapping, same as the measurement of EDX spectra, is limited by lower sensitivity to elements with lower atomic number.

6.2. Optical characterisation

UV–Vis spectroscopy is commonly used to characterise planar metal oxide CTLs on TCO substrates. It is not useful for mesoscopic layers or rough (nanorods with large diameters for example) layers due to significant scattering contribution. It represents a routine characterisation technique and it is not particularly informative if a suitable CTL is chosen, since typically wide band gap CTLs are used. In doped CTLs, it can be used to observe changes induced by doping, but even in that case it is just one in the array of indirect confirmation techniques that doping has made some difference, and it does not provide any direct evidence as to what exactly changed (states in the gap could be caused by increased concentration of native defects or by the dopant). Spectroscopic ellipsometry (SE) is a more comprehensive technique that can be used for both characterisation of the metal oxide layers, as well as the perovskite layer. For samples on transparent substrates such as glass, it should be paired with transmission measurements and the correction for the substrate back surface reflection should be employed (or the reflection from the back surface should be eliminated). Modelling of the ellipsometry data is nontrivial, and the technique has reasonable sensitivity so that acquiring good quality data on perovskite films in ambient could be challenging due to their sensitivity to ambient humidity (acquisition time is dependent on the type of instrument used, and the degradation rate is dependent on the humidity). Generally, SE is not commonly used unless device modelling is going to be attempted, where the knowledge on the index of refraction of each layer is needed.

Photoluminescence (PL) is commonly used for characterisation of the quality of the perovskite layer grown on metal oxide CTL and the charge transfer from the perovskite to the metal oxide CTL. Basic rationale is that efficient charge transfer from the perovskite to the metal oxide CTL will result in efficient luminescence quenching compared to the perovskite film on glass or ITO. Problematic part of this assumption is that the quality of the perovskite film, and consequently the concentration of non-radiative defects, is substrate dependent and thus quenching on a different substrate could occur due to a combination of the change in the quality of the perovskite layer and the charge transfer. In an attempt to understand better what is happening in the devices, time-resolved photoluminescence (TRPL) is commonly used in addition to PL. Effective minority carrier lifetime τ_{eff} can be obtained by fitting the TRPL decay curve with single/multiple exponential function or stretched exponential function, (see fitting details in [149]. and [150]). For perovskite layers on glass, longer PL lifetime is commonly used as an indicator of layer quality due to lower non radiative recombination [151], similar to higher intensity of the PL spectra. It was proposed that the effective photoluminescence decay time can be separated into bulk and surface contributions $1/\tau_{\text{eff}} = 1/\tau_{\text{bulk}} + 1/\tau_{\text{surface}}$, where the surface contribution contains components describing charge transfer at interface if any, and also non-radiative recombination losses at interface [17].

For perovskite layers on a CTL, biexponential fitting commonly yields so-called fast-decay and slow decay time constants [74]. However, interpretation of the fast and slow decay component can be complex due to various contributing factors, since the underlying layer below the perovskite alters its crystalline quality and interfacial trap density, in addition to luminescence decay due to charge transfer. Common interpretation of attributing the fast component to the charge transfer at the interface [152] and slow component to the radiative recombination in the bulk of the perovskite [45, 59] is likely incomplete, since it

does not take into account non-radiative recombination and/or charge trapping contributions at the interface. Thus, a method to extract more parameters with physical significance has been recently reported, including surface recombination/interface recombination velocity, monomolecular and bimolecular recombination constant, carrier mobility, and doping density [153]. In the absence of significant interfacial losses this simplified interpretation can be consistent with the other observed trends, but in some cases where simplified interpretation is insufficient, apparent contradictions with device performance trends could be observed [72]. In such cases, more comprehensive characterisation of charge dynamics may be necessary to understand what is actually happening in the devices. To provide an example of this, in NaCl treated NiO_x, NaCl treatment resulted in downward shift of NiO_x work function which should improve the charge extraction, but an increase in TRPL time constant was obtained for NaCl treatment [108]. From the device performance parameters (*FF*, V_{oc}) and electrical characterisation, it is obvious that charge extraction is improved and recombination is reduced, and thus increase in time constant can be attributed to reduced defects/defect passivation in the perovskite layer [108]. Similar observations can commonly occur for surface treatments/interfacial layers, since they tend to reduce interfacial defect density and/or improve the quality of the perovskite layer grown on top of the treated surface [107]. This nicely illustrates the need for combining the whole range of characterisation techniques to fully understand the effect of a dopant or surface treatment or interfacial layer on the device performance.

6.3. Electrical characterisation

Hall measurement is a widely-used technique to obtain the electrical properties of a conductive specimen with known thickness, such as charge carrier type, concentration, mobility, as well as sheet resistance and resistivity. Based on van der Pauw contact geometry [154], arbitrary shaped sample can be measured instead of requiring a micro-structured Hall bar, which typically requires photolithography procedure [155]. Theoretically, Hall measurement should be even easier for insulators due to their large Hall coefficient which is beneficial to obtain accurate carrier concentration value. However, in practice conducting Hall measurement on low-mobility (<1 cm^2 Vs^{-1}) polycrystalline thin film samples is challenging due to (1) the existence of large amount of grain boundaries laterally that result in the underestimated mobility by several orders of magnitude compared to the in-grain mobility and (2) the experimental limitations to detect the small Hall voltage signal, which is determined by the product of carrier mobility and magnetic field, i.e. $\mu \cdot \mathrm{B}$ [156]. While the first difficulty could be overcome by improved modelling [157], small values of Hall signal remain a problem, especially for instruments with the lower magnetic field strength. The measurement difficulties are particularly pronounced for very thin films of p-type materials, which must be deposited on non-conductive substrates (if deposited on ITO, observed behavior would be dominated by ITO), resulting in too small Hall voltages for measurement, even in instruments with 10 T magnetic field (instead of more common 1 T). A possible solution to this problem for thin films prepared by spin-coating nanoparticles is to compress nanoparticles into a pellet and then perform Hall measurement [89]. However, this approach may also result in experimental difficulties depending on whether nanoparticles could form a pellet which could be handled, or compressed particles would simply be too fragile and pellet would readily fall apart. In addition, alternative Current Hall Effect techniques have been developed and achieved improved sensitivity to Hall voltage [158,159] to characterize low-mobility materials, but they exhibit other problems, such as the interpretation, electronics setup, and the treatment of parasitic resistances and capacitances [156]. Another alternative method of electrical characterisation is to measure the sheet resistance using a Four Point Probe Resistance Tester then calculating its resistivity with measured thickness, which is also valid to low-conductivity specimen due to the absence of magnetic field and Hall signals.

Furthermore, conductive AFM (C-AFM) can provide electrical [160] and morphological [161] information of low-conductivity oxide thin films, using a conductive tip and a voltage bias. In a C-AFM measurement, the current flow direction is vertically from C-AFM tip to thin film specimen to conductive substrate to sample stage, thus it is straightforward to measure oxide thin-films with a nanoscale thickness. As the tip scans on the sample surface, in-grain and grain boundary areas respond differently, so the conductivity distribution can be directly obtained. The measured current I obeys the relationship of $I = J \times A_{\mathrm{eff}}$, where J is the current density, A_{eff} is the effective emission area [160, 162]. Apparently smaller A_{eff} provides higher lateral resolution and lower conductivity materials show smaller A_{eff}. The value of A_{eff} is also significantly affected by atmosphere condition, such as humidity and vacuum degree, and it can range from 1 n m^2 in ultra-high vacuum to 300 n m^2 in humid air [163].

In addition to these basic techniques which are commonly used to evaluate the conductivity change of the CTL with the surface treatment, the change of deposition conditions, and/or the introduction of dopant, it is necessary to evaluate defects at interfaces, and examine the recombination losses in the devices. One of the most straightforward methods to do so is to determine the diode ideality factor n_{id} by measuring the dependence of open circuit voltage on illumination power P, since this measurement does not require altered

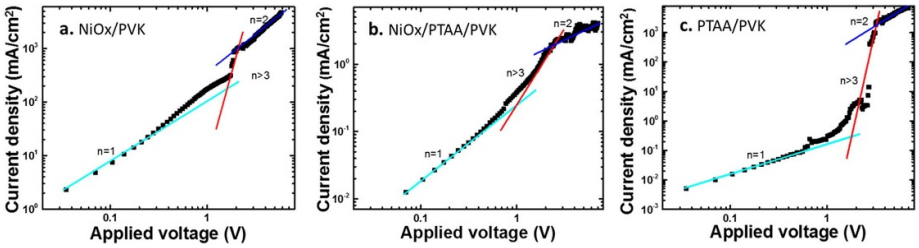

Figure 6. Trap state density measurements by dark I–V curve of a perovskite film grown on NiO_x (a), NiO_x/PTAA (b), and PTAA-coated FTO/ glass (c). The basic structure for this measurement is FTO/HTM/PVK/HTM/Au where the structure is FTO/NiO_x/PVK/PTAA/Au for (a), FTO/NiO_x/PTAA/PVK/PTAA/Au for (b), and FTO/PTAA/PVK/PTAA/Au for (c). Reproduced with permission from [104].

device configuration nor special equipment (other than neutral density filters to change the optical power of the solar simulator. The ideality factor is described as:

$$V_{oc} = \frac{E_g}{q} - \frac{n_{id}k_BT}{q}\ln\frac{P_0}{P}, \tag{1}$$

where E_g is the absorber band gap, k is Boltzmann constant, T is the temperature, and P_0 refers full intensity of illumination [164]. Lower n_{id} value close to ideal value of 1 is generally desired, since it indicates a lower contribution of trap-assisted Shockley-Read-Hall (SRH) recombination [165]. However, it should be noted that in this case as well careful interpretation of the measured data is needed. For example, a low V_{oc} was reported in a device with $n_{id} = 1$ [166]. That is because that the low n_{id} value could also result from surface recombination due to non-selective contacts and the shape of V_{oc}-light intensity plot may help to evaluate the recombination situation [164]. Thus, while generally n_{id} closer to one is considered to be desirable and a useful measure of the recombination losses in the devices [108], due to the complexity of phenomena contributing to overall device performance it is always highly desirable to perform different measurements for comprehensive optical and electrical characterisation and then examine whether conclusions consistent with all the measurement results could be obtained.

Useful information on the recombination can also be obtained from transient photovoltage measurements, where slower decay was claimed to indicate suppressed recombination [43, 75]. Transient photocurrent measurements are a useful complementary technique, providing useful information on charge collection (faster decay, more efficient charge collection) [75]. However, careful interpretation of transient electrical measurements is needed, because they are also affected by the capacitance of the devices. Thus, it is always advisable to use multiple techniques together to cross-check whether the trends observed from all the techniques are consistent with the conclusion drawn.

In addition, to determine the trap density at the CTL/perovskite interface, *I–V* curves for electron-only (for ETLs) or hole-only (for HTLs) devices are often measured. Based on the space charge limited current (SCLC) model, the *I–V* curve will consist of a linear ohmic response region (at low voltages), followed by the trap filling regime, and then SCLC regime at higher bias voltages [44]. This allows the determination of the trap density N_t from the trap-filled limit voltage V_{TFL}, which denotes the transition from linear ohmic to high slope trap-filling regime [44, 45]. The trap density can then be determined as $N_t = (2\epsilon\epsilon_0/eL^2)V_{\mathrm{TFL}}$, where ε is the dielectric constant of the perovskite, ε_0 is the vacuum permittivity, L is the thickness of the perovskite film, and e is elementary charge [44, 45]. Obviously, the accuracy of the estimated trap density will depend on the accuracy of determined V_{TFL}, as well as the thickness of the perovskite film. Both of these factors can contribute to difficulties in getting a correct estimate of the trap density. If estimating the thickness from cross-section SEM or TEM images, taking multiple measurements and determining averages is highly advisable, as well as making sure that no distortions have been introduced by sample preparation. While a simpler method could be the use of step-profiler, one would expect that in a relatively soft material such as perovskite, thickness estimate errors could occur, similar to organic layers. As for V_{TFL}, the accuracy of estimate would depend on the shape of the *I–V* curve, i.e. the existence of a clear transition between different current regimes. One example of the use of *I–V* characteristics to determine the trap density is shown in figure 6 [104]. It can be observed that in some cases a clear region where $n > 3$ cannot be determined. Even more drastic case is demonstrated in figure 7 [167], where the transition between regimes can barely be observed, resulting in a large uncertainty of then determined V_{TFL}. The figure also illustrates another example of data where model does not fit, i.e. statistical distribution of performance cannot be described by a Gaussian distribution. In cases where the data do not fit the theoretical model, it is advisable

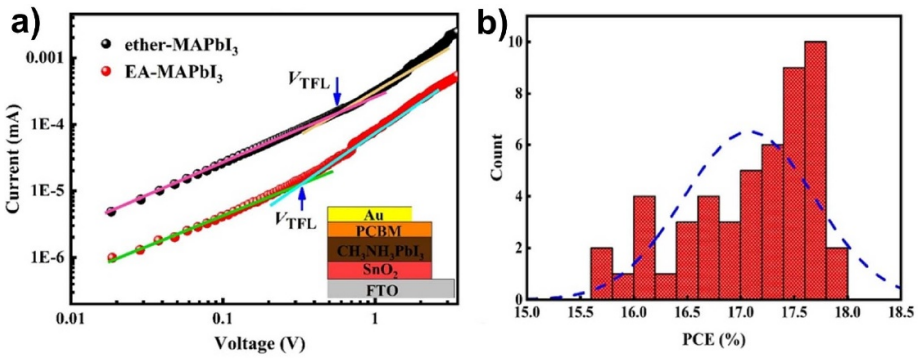

Figure 7. (a) Dark current–voltage curves of the electron-only devices showing V_{TFL} kink point behavior, the inset displays the device structure. (b) Histograms of photovoltaic PCEs from 50 devices. Reproduced with permission from [167].

to examine possible reasons for the discrepancy. For example, it is sometimes possible to improve the quality of the data by eliminating excess ITO/FTO from the substrate pattern and by making sure individual devices on the substrate are electrically isolated (for example by laser etching, or by simply making one device per substrate), or by choosing a different top CTL to ensure that devices are truly single-carrier devices where the model is valid. If this approach fails and the *I–V* curve still does not exhibit a clear shape consistent with trap-filled regime, it would be appropriate to obtain the information on the density of traps from other measurements, such as Mott-Schottky plots. In general, the estimates of trap density from Mott-Schottky plots are advisable for cross-checking, though in that case as well thickness determination uncertainties could affect the accuracy of the number obtained, but similar error would be introduced for two methods, affecting possible comparisons with other literature reports but ensuring internal consistency. It should also be noted that differences observed in the estimated interface trap densities in different literature reports of cells with similar efficiencies could likely be attributed to the uncertainties in estimates of either L or V_{TFL}. Nevertheless, the method is still highly useful for relative comparisons between, for example, devices with modified and un-modified CTL/perovskite interfaces in the same manuscript.

Mott-Schottky (MS) analysis is a capacitance based method to extract parameters such as trap [168] (or doping [169]) density N in depletion zone, built-in voltage V_{bi} and depletion layer width w, through measuring the capacitive response to an input sweeping DC bias with small-amplitude constant-frequency AC component overlapped. V_{bi} and N can be extracted from the Mott-Schottky equation:

$$\frac{1}{C_{dl}^2} = \frac{2(V_{bi} - V)}{\epsilon\epsilon_0 q A^2 N}, \tag{2}$$

where ϵ, ϵ_0, q, A is the vacuum permittivity, relative dielectric constant of perovskite, elementary charge, active area, respectively. Higher V_{bi} is preferred, for higher likelihood to obtain larger V_{oc} [170, 171], larger J_{sc}, [171] faster charge transport and collection [171, 172], reduced trap states [172], and/or less charge accumulation at interfaces [172]. Higher N value either indicates more defects [173] or effective doping [174] depending on the application scenario. MS analysis under illumination [175, 176], liquid electrolyte condition [177], different temperatures [178], can also be studied. Further, it should be noted that the obtained V_{bi} and trap (doping) density N would be invalid if improper frequency is applied or perovskite film has sufficiently low defects density ($<10^{17}$ cm^{-3}), since there would be no distinguishable C_{dl} (depletion layer capacitance) region for MS analysis [179]. For frequency selection, it is recommended to measure capacitance as a function of frequency, and a proper frequency should be in the dielectric polarization plateau region which corresponds to the depletion zone [179]. However, many published MS plots did not show distinguishable C_{dl} zone [168, 170, 171]. Thus, same as with other techniques discussed, combination of techniques and careful interpretation of the results are needed to draw valid conclusions. If all the techniques give internally consistent results, it is more likely that the obtained conclusions are valid.

In addition to the total trap density. We can also estimate the distribution of trap density of states from MS measurements according to the formula [107]:

$$tDOS(E_\omega) = -\frac{V_{bi}}{qW}\frac{dC}{d\omega}\frac{\omega}{kT}, \tag{3}$$

where T is the temperature, k is Boltzmann constant, q is elementary charge, W is the depletion width, C is the capacitance, and ω is the angular frequency. It is common to observe two peaks in tDOS, with shallower

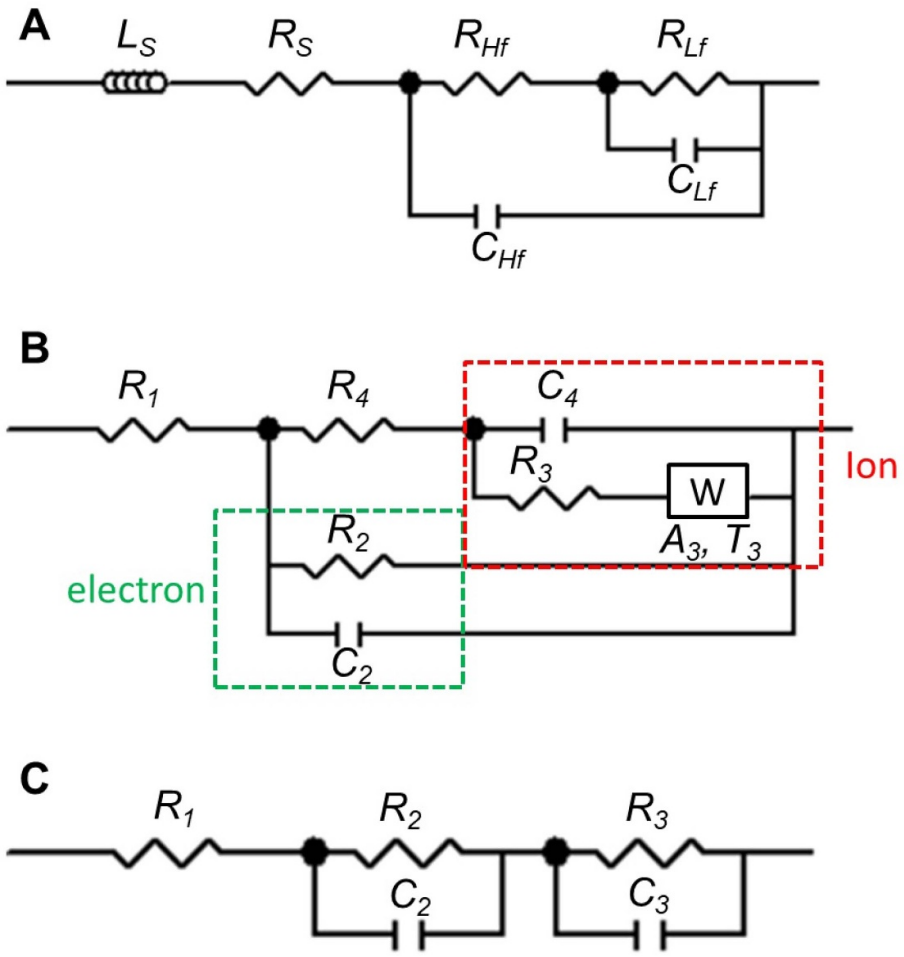

Figure 8. (a) Complete equivalent circuit for modelling EIS measurements of PSCs [182]. (b) Equivalent circuit separating electron and ion contributions [188]. (c) Equivalent circuit commonly used in PSCs [50, 123].

energy peak (around 0.35–0.40 eV) commonly assigned to grain boundary traps, while the deeper one (around 0.4–0.52 eV) has been commonly assigned to surface traps [107].

Finally, another common electrical characterisation technique is Electrochemical Impedance Spectroscopy (EIS) or Impedance Spectroscopy (IS). EIS is an in-situ frequency domain technique that can distinguish various relaxation processes due to their different time scales, including charge transport in bulk materials, charge transfer at interfaces, and charge recombination [180, 181]. EIS can provide the values of coupled capacitive-resistive (RC) and other elements by equivalent circuit model (ECM) fitted Nyquist plot, as well as permittivity of perovskite by capacitance-frequency spectrum in full depletion region [180].

Various ECMs have been proposed to describe the underlying physical phenomena present [182–184]. A commonly reported ECM is shown in figure 8 [182], where L_S and R_S are caused by wires and connections, the high frequency capacitance C_{Hf} is associated with the geometric capacitance C_g, while the high frequency capacitance C_{Lf} is ascribed to chemical capacitance C_μ [185]. C_g is produced by the electrical field between two charge contacts, referring to the dielectric property of perovskite [186], while C_μ reflects the capability to accept or release additional carriers due to the change in their chemical potential [183]. To obtain more useful insights, performing EIS as a function of different parameters, such as dc voltage bias, illumination, temperature, variation of contact materials, etc is of interest [180]. In some cases, other equivalent circuit models are used, or elements of the equivalent circuit for which no evidence exists in the measured data, such as L_S, are left out [108].

In EIS measurement of an efficient PSC, typically two semi-circles are obtained, with the semi-circle in high frequency region attributed to charge transfer and transport resistance R_{ct}, while the semi-circle in low frequency region is attributed to the recombination resistance R_{rec} [41]. Thus, the common ECM includes series resistance connected in series to two parallel circuits consisting of a resistance and capacitance or capacitive element [50, 123], as shown in figure 8(c). The obtained resistance values can provide information about charge extraction and charge recombination, and they can be determined at different applied voltages

[41] and/or under illumination [49, 77]. However, there have been different models used in the literature, and different interpretations. For example, estimate of the recombination resistance by adding the resistances for high and low frequency semicircles in Nyquist plot has also been reported [53]. In addition, a single semi-circle is sometimes observed (though this is more common in devices with efficiency below 20%) and then a single resistor-capacitor parallel circuit is used in the equivalent circuit model [74, 75, 100]. The lack of consensus and differences in interpretation of EIS results have been acknowledged in the literature [187]. Nevertheless, it was claimed that despite the complexity of the phenomena, which have been discussed in detail, the technique could be used to provide semi-quantitative and qualitative information on the nature of recombination processes [187]. However, since it has been claimed that inconsistencies in the interpretation of low frequency arc are likely due to the ionic movement [187], it would be helpful to include ionic motion in the models. A suitable model to take into account both ionic and electronic contribution has been recently proposed [188], as illustrated in figure 8(b). It remains to be seen if this model will become more widely adopted, and if it will be further refined upon its wider application to a greater variety of devices exhibiting different behaviours.

In addition to these techniques, other less common characterisations can be helpful, such as time resolved microwave conductivity [48], photo thermal deflections spectroscopy (PDS) [189], low frequency noise measurements [189], etc, can be potentially useful to provide more detailed information on charge transport, trap states, and implications on charge collection. They are likely less common due to equipment being less common in research groups working on PSCs, but they can nevertheless have some advantages over conventional characterisation methods. For example, PDS has higher sensitivity compared to absorption spectroscopy to characterise disorder and states within the gap [189]. Generally, it is highly desirable to use multiple characterisation techniques to derive conclusions on how the choice of the CTL or its surface treatment or interfacial layer affects the charge collection and charge recombination, since the phenomena contributing to charge collection and recombination are complex and the use of any single technique is not sufficiently conclusive. Nevertheless, even a combination of experimental techniques can, in some specific cases, return results which do not accurately describe recombination dynamics [190]. In those cases, device numerical simulations may be needed to fully understand charge transport and charge recombination processes [190].

7. Conclusions and future outlook

In this review, we have discussed the use of metal oxides in PSCs, focusing on approaches involving low temperature processing and/or yielding high performance devices. It should be noted though that some of the reports achieving lower efficiencies (16%–18%) have potential for significant efficiency improvements (to 18–20% range) by switching the active layer from $MAPbI_3$ to mixed cation perovskite. Nevertheless, the use of mixed cation perovskites would likely require separate optimisation of the interface and perovskite deposition process, which is beyond the scope of this review. Generally, while lots of progress has been made, there is still lots of opportunity for further improvement and unsolved problems, in particular when it comes to devices using metal oxides as both CTLs. What can be identified as a definite trend is that combinations of different approaches and optimisation of all interfaces in the devices and the elimination of less stable materials is the likely way forward towards high efficiency, high stability devices.

Different approaches investigated, namely the modifications of the deposition methods and/or deposition conditions of metal oxide CTLs, doping, surface treatments, interface modifications and/or interfacial layers aiming to improve PSC performance typically work based on the following mechanisms: (a) improved charge collection, (b) reduced interfacial traps/reduced recombination losses, (c) improved quality of the perovskite layer deposited on top of the CTL. We have provided an overview of different experimental techniques that can be used to distinguish which of these mechanisms contribute to the improved performance of the devices. Improved charge collection should be primarily evident from improved short circuit current density J_{sc}, and verified by more favourable energy alignment between the perovskite and CTL as evidenced by UPS and/or KPFM (at least one of these techniques is a must), PL and TRPL (careful interpretation of the fitting results is necessary), and photocurrent transients. Reduced interfacial defects and/or reduced recombination losses should be primarily evident from improved fill factor (FF), and verified by determination of trap density from V_{TFL} measurements, Mott-Schottky plots, EIS measurements (careful selection of equivalent circuit and interpretation of fitted parameters are necessary), and/or diode ideality factor determination from the dependence of the open circuit voltage on the illumination power, and photovoltage transients. Multiple characterisation techniques are preferred for consistent results. Finally, improved quality of the perovskite layer can be verified by GIWAXS, PL and TRPL, and can be complemented by PDS and low frequency noise measurements. In some cases, useful information can be obtained from morphological characterisation (SEM, AFM) and examination of contact angle of the

perovskite solution on modified and unmodified surfaces. However, it should be noted that it is not uncommon that morphological examination does not show significant differences among films having large differences in device performance.

Finally, we would like to emphasize the need for not only comprehensive characterisation of the devices to fully understand the mechanisms for the observed trends, but also the need for more comprehensive stability testing. The trend in the field remains to be reporting the stability for dark storage, while there is increasing need for stability testing using various accelerated ageing protocols (for a complete list of adapted ISOS protocols for PSCs, see [12]) and outdoor testing. Yet, outdoor tests remain almost as scarce as reports on metal oxide CTLs on both sides of the perovskite layer, despite the fact that performing ISOS-O1 protocol at open circuit is quite straightforward and it simply involves encapsulating the devices and mounting them at a suitable angle outdoors and testing them periodically in the lab. However, this would require stable encapsulation, which is particularly challenging for outdoor tests due to intrinsic thermal cycling involved in outdoor testing due to exposure to weather, which can be problematic for common approaches using epoxies and cover glass. Possible solution to the problem would be metal oxide barrier layers (preferably deposited by ALD) combined with cover glass and edge sealant approach, so that further investigation of metal oxide barrier layers would definitely be of interest, combined with wider adoption of standardised stability testing protocols.

Data availability statement

Data sharing is not applicable to this article as no new data were created or analyzed in this study.

Acknowledgments

Financial support from the Seed Funding for Strategic Interdisciplinary Research Scheme of the University of Hong Kong and Shenzhen Science and Technology Commission Projects Nos. JCYJ20160530184523244 and JCYJ20170818141216288 is acknowledged Z B thanks the support from the Shenzhen Key Laboratory Project (No. ZDSYS201602261933302).

ORCID iDs

Aleksandra B Djurišić https://orcid.org/0000-0002-5183-1467
Alan Man Ching Ng https://orcid.org/0000-0001-7081-8244

References

[1] Yin X, Zhai J, Song L, Du P, Li N, Yang Y, Xiong J and Ko F 2019 *ACS Appl. Mater. Interfaces* **11** 44308–14
[2] Li G, Deng K, Dou Y, Liao Y, Wang D, Wu J and Lan Z 2019 *Sol. Energy* **193** 111–17
[3] Wang Q *et al* 2020 *Adv. Mater. Interfaces* **7** 1901866
[4] Song J, Li G, Wang D, Sun W, Wu J and Lan Z 2020 *Sol. RRL* **4** 1900558
[5] Roose B, Wang Q and Abate A 2019 *Adv. Energy Mater.* **9** 1803140
[6] Wang P, Li R, Chen B, Hou F, Zhang J, Zhao Y and Zhang X 2020 *Adv. Mater.* **32** 1905766
[7] Jiang Q *et al* 2019 *Nat. Photon.* **13** 460–6
[8] Zheng X *et al* 2020 *Nat. Energy* **5** 131–40
[9] Yang D, Yang R, Priya S and Liu S F 2019 *Angew. Chem. Int. Ed.* **58** 4466–83
[10] Mujahid M, Chen C, Hu W, Wang Z-K and Duan Y 2020 *Sol. RRL* **4** 1900556
[11] Boyd C C, Cheacharoen R, Leijtens T and McGehee M D 2019 *Chem. Rev.* **119** 3418–51
[12] Khenkin M V *et al* 2020 *Nat. Energy* **5** 35–49
[13] Nie W *et al* 2018 *Adv. Mater.* **30** 1703879
[14] He Q, Yao K, Wang X, Xia X, Leng S and Li F 2017 *ACS Appl. Mater. Interfaces* **9** 41887–97
[15] Yao K *et al* 2019 *Joule* **3** 417–31
[16] Li R, Wang P, Chen B, Cui X, Ding Y, Li Y, Zhang D, Zhao Y and Zhang X 2019 *ACS Energy Lett.* **5** 79–86
[17] Wang J, Fu W, Jariwala S, Sinha I, Jen A K Y and Ginger D S 2019 *ACS Energy Lett.* **4** 222–7
[18] Haque M A, Sheikh A D, Guan X and Wu T 2017 *Adv. Energy Mater.* **7** 1602803
[19] Noh M F M *et al* 2018 *J Mater. Chem.* C **6** 682–712
[20] Flannery L, Galvez H, Nimens W, Rahman A A and Whittaker-Brooks L 2019 *Polyhedron* **170** 334–58
[21] Guai G H, Song Q L, Lu Z S and Li C-M 2011 *Surf. Coat. Tech.* **205** 2852–6
[22] Jiang Q, Zhang X and You J 2018 *Small* **14** 1801154
[23] McCarthy M M *et al* 2018 *MRS Adv.* **3** 3075–84
[24] Jeong S, Seo S, Park H and Shin H 2019 *Chem. Commun.* **55** 2433–6
[25] Hu T *et al* 2017 *Adv. Mater.* **29** 1606656
[26] Kam M, Zhang Q, Zhang D and Fan Z 2019 *Sci. Rep.* **9** 6963
[27] Shi X, Chen R, Jiang T, Ma S, Liu X, Ding Y, Cai M, Wu J and Dai S 2020 *Sol. RRL* **4** 1900198
[28] Yang G *et al* 2018 *Adv. Mater.* **30** 1706023

[29] Chen D et al 2019 Sol. Energy 188 239–46
[30] Ren J et al 2019 ChemElectroChem 6 3167–74
[31] Zhang P et al 2018 Adv. Mater. 30 1703737
[32] Luo C-Q et al 2019 Appl. Surf. Sci. 483 1129–35
[33] Son D, Moon B J, Lee A, Rho H, Lee H J, Kim T-W, Ha J-S and Lee S H 2019 Appl. Surf. Sci. 483 165–9
[34] Yan L et al 2018 Adv. Mater. 30 1802509
[35] Ma J, Su J, Lin Z, Zhou L, He J, Zhang J, Liu S, Chang J and Hao Y 2020 Nano Energy 67 104241
[36] Turren-Cruz S-H et al 2018 Energy Environ. Sci. 11 78–86
[37] Yang D et al 2018 Nat. Commun. 9 3239
[38] Liu K, Chen S, Wu J, Zhang H, Qin M, Lu X, Tu Y, Meng Q and Zhan X 2018 Energy Environ. Sci. 11 3463–71
[39] Tavakoli M M, Saliba M, Yadav P, Holzhey P, Hagfeldt A, Zakeeruddin S M and Graetzel M 2019 Adv. Energy Mater. 9 1802646
[40] Zhu P, Gu S, Luo X, Gao Y, Li S, Zhu J and Tan H 2020 Adv. Energy Mater. 10 1903083
[41] Chen J, Zhao X, Kim S-G and Park N-G 2019 Adv. Mater. 31 1902902
[42] Singh M, Ng A, Ren Z, Hu H, Lin H-C, Chu C-W and Li G 2019 Nano Energy 60 275–84
[43] Liu Z, Deng K, Hu J and Li L 2019 Angew. Chem. Int. Ed. 58 11497–504
[44] Cao T, Chen K, Chen Q, Zhou Y, Chen N and Li Y 2019 ACS Appl. Mater. Interfaces 11 33825–34
[45] Zhang X et al 2019 J Mater. Chem. A 7 22323–31
[46] Lee Y et al 2018 Adv. Sci. 5 1800130
[47] Lee J H et al 2019 J. Phys. Chem. Lett. 10 6545–50
[48] Noel N K, Habisreutinger S N, Wenger B, Lin Y-H, Zhang F, Patel J B, Kahn A, Johnston M B and Snaith H J 2020 Adv. Energy Mater. 10 1903231
[49] Zhao X et al 2018 Nano Lett. 18 2442–9
[50] Cao Q, Li Z, Han J, Wang S, Zhu J, Tang H, Li X and Li X 2019 Sol. RRL 3 1900333
[51] Akin S 2019 ACS Appl. Mater. Interfaces 11 39998–40005
[52] Zhu N et al 2019 ACS Appl. Energy Mater. 2 3676–82
[53] Fabiola Mendez P, Muhammed S K M, Barea E M, Masi S and Mora-Sero I 2019 Sol. RRL 3 1900191
[54] Savva A, Burgues-Ceballos I and Choulis S A 2016 Adv. Energy Mater. 6 1600285
[55] Spalla M, Planes E, Perrin L, Matheron M, Berson S and Flandin L 2019 ACS Appl. Energy Mater. 2 7183–95
[56] Seitkhan A et al 2020 Adv. Funct. Mater. 30 2004273
[57] Noh Y W, Lee J H, Jin I S, Park S H and Jung J W 2019 Nano Energy 65 104014
[58] Tu B et al 2019 Adv. Mater. 31 1805944
[59] Wang D, Chen S-C and Zheng Q 2019 J. Mater. Chem. C 7 12204–10
[60] Liu C, Zhang D, Li Z, Han W, Ren G, Li Z, Shen L, Guo W and Zheng W 2020 Sol. RRL 4 1900489
[61] Tavakoli M M, Tavakoli R, Yadav P and Kong J 2019 J. Mater. Chem. A 7 679–86
[62] Cao J, Wu B, Chen R, Wu Y, Hui Y, Mao B-W and Zheng N 2018 Adv. Mater. 30 1705596
[63] Ma J et al 2017 Adv. Sci. 4 1700031
[64] Wang J, Datta K, Weijtens C H L, Wienk M M and Janssen R A J 2019 Adv. Funct. Mater. 29 1905883
[65] Wang P et al 2018 J. Mater. Chem. A 6 15853–8
[66] Dagar J, Hirselandt K, Merdasa A, Czudek A, Munir R, Zu F, Koch N, Dittrich T and Unger E L 2019 Sol. RRL 3 1900088
[67] Guo Z, Teo S, Xu Z, Zhang C, Kamata Y, Hayase S and Ma T 2019 J. Mater. Chem. A 7 1227–32
[68] Tian J et al 2019 Adv. Mater. 31 1901152
[69] Hong J A et al 2020 ACS Appl. Mater. Interfaces 12 2417–23
[70] Mohamadkhani F, Javadpour S and Taghavinia N 2019 Sol. Energy 191 647–53
[71] Zhang X et al 2020 Adv. Funct. Mater. 30 1910530
[72] Guo Y, Lei H, Wang C, Ma J, Chen C, Zheng X, Yang G, Xiong L and Tan Z 2020 Sol. RRL 4 1900482
[73] Li X, Yang J, Jiang Q, Chu W, Xin J, Hou J and Lai H 2018 Electrochim. Acta 261 474–81
[74] Deng Y, Li S, Li X, Wang R and Li X 2019 Electrochim. Acta 326 134924
[75] Zhu W, Chai W, Zhang Z, Chen D, Chang J, Liu (Frank) S, Zhang J, Zhang C and Hao Y 2019 Org. Electron. 74 103–9
[76] Hui W et al 2020 Adv. Mater. 32 1906374
[77] Tang H et al 2020 Sol. RRL 4 1900415
[78] Pang A, Shen D, Wei M and Chen Z-N 2018 ChemSusChem 11 424–31
[79] Sun C, Guan L, Guo Y, Fang B, Yang J, Duan H, Chen Y, Li H and Liu H 2017 J. Alloys Compd. 722 196–206
[80] Hou Q et al 2018 ChemElectroChem 5 726–31
[81] Chen C et al 2020 Sol. RRL 4 1900499
[82] Huang Z, Ouyang D, Shih C-J, Yang B and Choy W C H 2019 Adv. Energy Mater. 10 1900903
[83] Di Girolamo D et al 2019 Adv. Energy Mater. 9 1901642
[84] Yates H M, Meroni S M P, Raptis D, Hodgkinson J L and Watson T M 2019 J Mater. Chem. C 7 13235–42
[85] Qin Y, Song J, Qiu Q, Liu Y, Zhao Y, Zhu L and Qiang Y 2019 J. Alloys Compd. 810 151970
[86] Lee S, Roh H-S, Han G S and Lee J-K 2019 Nano Res. 12 3089–94
[87] Di Girolamo D, Matteocci F, Piccinni M, Di Carlo A and Dini D 2020 Sol. Energy Mater. Sol. Cells 205 110288
[88] Sun J, Lu J, Li B, Jiang L, Chesman A S R, Scully A D, Gengenbach T R, Cheng Y-B and Jasieniak J J 2018 Nano Energy 49 163–71
[89] Chen W et al 2018 Adv. Energy Mater. 8 1703519
[90] Li G, Jiang Y, Deng S, Tam A, Xu P, Wong M and Kwok H-S 2017 Adv. Sci. 4 1700463
[91] Liu Z, Chang J, Lin Z, Zhou L, Yang Z, Chen D, Zhang C, Liu S F and Hao Y 2018 Adv. Energy Mater. 8 1703432
[92] Singh A, Ranjan R, Ranjan S, Singh A, Garg A and Gupta R K 2020 J. Nanosci. Nanotechnol. 20 3710–17
[93] Lin Y-R, Liao Y-S, Hsiao H-T and Chen C-P 2020 Appl. Surf. Sci. 504 144478
[94] Ullrich F et al 2018 ACS Appl. Energy Mater 1 3113–22
[95] Chakrabarti S, Carolan D, Alessi B, Maguire P, Svrcek V and Mariotti D 2019 Nanoscale Adv. 1 4915–25
[96] Xu L, Liang H-W, Yang Y and Yu S-H 2018 Chem. Rev. 118 3209–50
[97] Wan X, Jian Y, Qiu Z, Zhang H, Zhu X, Sikandar I, Liu X, Chen X and Cao B 2018 ACS Appl. Energy Mater. 1 3947–54
[98] Saki Z, Sveinbjoernsson K, Boschloo G and Taghavinia N 2019 ChemPhysChem 20 3322–7
[99] Chen W, Liu F-Z, Feng X-Y, Djurisic A B, Chan W K and He Z-B 2017 Adv. Energy Mater. 7 1700722
[100] He J, Xiang Y, Zhang F, Lian J, Hu R, Zeng P, Song J and Qu J 2018 Nano Energy 45 471–9

[101] Xu L, Chen X, Jin J, Liu W, Dong B, Bai X, Song H and Reiss P 2019 *Nano Energy* **63** 103860
[102] Ru P *et al* 2020 *Adv. Energy Mater.* **10** 1903487
[103] Chen W *et al* 2018 *Adv. Mater.* **30** 1800515
[104] Du Y, Xin C, Huang W, Shi B, Ding Y, Wei C, Zhao Y, Li Y and Zhang X 2018 *ACS Sustain. Chem. Eng.* **6** 16806–12
[105] Zhang J *et al* 2018 *Nanoscale* **10** 5617–25
[106] Xue Q *et al* 2017 *Adv. Energy Mater.* **7** 1602333
[107] Chen W *et al* 2019 *Adv. Energy Mater.* **9** 1803872
[108] Di Girolamo D *et al* 2019 *Adv. Mater. Interfaces* **6** 1900789
[109] Tan W, Hendricks O L, Meng A C, Braun M R, McGehee M D, Chidsey C E D and McIntyre P C 2018 *Adv. Mater. Interfaces* **5** 1800191
[110] Yang B, Ouyang D, Huang Z, Ren X, Zhang H and Choy W C H 2019 *Adv. Funct. Mater.* **29** 1902600
[111] Huang Z, Ouyang D, Ma R, Wu W, Roy V A L and Choy W C H 2019 *Adv. Funct. Mater.* **29** 1904684
[112] Ouyang D, Xiao J, Ye F, Huang Z, Zhang H, Zhu L, Cheng J and Choy W C H 2018 *Adv. Energy Mater.* **8** 1702722
[113] Papadas I T, Ioakeimidis A, Armatas G S and Choulis S A 2018 *Adv. Sci.* **5** 1701029
[114] Yi H, Wang D, Duan L, Haque F, Xu C, Zhang Y, Conibeer G and Uddin A 2019 *Electrochim. Acta* **319** 349–58
[115] Bashir A *et al* 2018 *Nanoscale* **10** 2341–50
[116] Liu C, Zhou X, Chen S, Zhao X, Dai S and Xu B 2019 *Adv. Sci.* **6** 1801169
[117] You J *et al* 2016 *Nat. Nanotech.* **11** 75
[118] Mali S S, Patil J V, Kim H, Luque R and Hong C K 2019 *Mater. Today* **26** 8–18
[119] Cao J, Yu H, Zhou S, Qin M, Lau T-K, Lu X, Zhao N and Wong C-P 2017 *J. Mater. Chem.* A **5** 11071–7
[120] Chiang Y-H, Shih C-K, Sie A-S, Li M-H, Peng C-C, Shen P-S, Wang Y-P, Guo T-F and Chen P 2017 *J. Mater. Chem.* A **5** 25485–93
[121] Wang Y, Wu Y, Gong L, Zhou N and Jiang M 2018 *J. Photon. Energy* **8** 025503
[122] Icli K C and Ozenbas M 2018 *Electrochim. Acta* **263** 338–45
[123] Liu Z, Zhu A, Cai F, Tao L, Zhou Y, Zhao Z, Chen Q, Cheng Y-B and Zhou H 2017 *J. Mater. Chem.* A **5** 6597–605
[124] Kaneko R, Kanda H, Sugawa K, Otsuki J, Islam A and Nazeeruddin M K 2019 *Sol. RRL* **3** 1900172
[125] Subbiah A S, Mahuli N, Agarwal S, van Hest M F and Sarkar S K 2017 *Energy Technol.* **5** 1800–6
[126] Hultqvist A, Aitola K, Sveinbjornsson K, Saki Z, Larsson F, Torndahl T, Johansson E, Boschloo G and Edoff M 2017 *ACS Appl. Mater. Interfaces* **9** 29707–16
[127] Lv Y *et al* 2018 *ACS Appl. Mater. Interfaces* **10** 23928–37
[128] Yang Y, Zhu Y, Wang X, Song Q, Ji C, Zhang H, He Z and Liang C 2020 *Int. J. Photoenergy* **2020** 5039192
[129] Singh R, Ghosh S, Subbiah A S, Mahuli N and Sarkar S K 2020 *Sol. Energy Mater. Sol. Cells* **205** 110289
[130] Hou Y *et al* 2017 *Science* **358** 1192
[131] Raiford J A, Boyd C C, Palmstrom A F, Wolf E J, Fearon B A, Berry J J, McGehee M D and Bent S F 2019 *Adv. Energy Mater.* **9** 1902353
[132] Wang Y, Mahmoudi T, Rho W-Y, Yang H-Y, Seo S, Bhat K S, Ahmad R and Hahn Y-B 2017 *Nano Energy* **40** 408–17
[133] Wang Y, Mahmoudi T, Yang H-Y, Bhat K S, Yoo J-Y and Hahn Y-B 2018 *Nano Energy* **49** 59–66
[134] Yin X, Zhai J, Wang T, Jing W, Song L, Xiong J and Ko F 2019 *ACS Appl. Mater. Interfaces* **11** 12460–6
[135] Yang Y, Chen H, Zheng X, Meng X, Zhang T, Hu C, Bai Y, Xiao S and Yang S 2017 *Nano Energy* **42** 322–33
[136] Luo Q *et al* 2017 *Adv. Funct. Mater.* **27** 1703068
[137] Sajid S, Elseman A M, Wei D, Ji J, Dou S, Huang H, Cui P and Li M 2019 *Nano Energy* **55** 470–6
[138] Tan K W, Moore D T, Saliba M, Sai H, Estroff L A, Hanrath T, Snaith H J and Wiesner U 2014 *ACS Nano* **8** 4730–9
[139] Kim Y *et al* 2017 *Energy Environ. Sci.* **10** 2109–16
[140] Zhang J, Mao W, Duan J, Huang S, Zhang Z, Ou-Yang W, Zhang X, Sun Z and Chen X 2019 *Electrochim. Acta* **318** 384–91
[141] Tang G *et al* 2019 *Adv. Mater.* **31** 1807689
[142] Qin M *et al* 2019 *Adv. Mater.* **31** 1901284
[143] Harvey S P, Li Z, Christians J A, Zhu K, Luther J M and Berry J J 2018 *ACS Appl. Mater. Interfaces* **10** 28541–52
[144] Christians J A, Schulz P, Tinkham J S, Schloemer T H, Harvey S P, de Villers B J T, Sellinger A, Berry J J and Luther J M 2018 *Nat. Energy* **3** 68–74
[145] Liu Y, Lorenz M, Ievlev A V and Ovchinnikova O S 2020 *Adv. Funct. Mater.* **30** 2002201
[146] Harvey S P, Zhang F, Palmstrom A, Luther J M, Zhu K and Berry J J 2019 *ACS Appl. Mater. Interfaces* **11** 30911–18
[147] Zhou Y, Sternlicht H and Padture N P 2019 *Joule* **3** 641–61
[148] Kosasih F U and Ducati C 2018 *Nano Energy* **47** 243–56
[149] Tang L, Ji R, Li X, Teng K S and Lau S P 2013 *J. Mater. Chem.* C **1** 4908–15
[150] de Quilettes D W, Vorpahl S M, Stranks S D, Nagaoka H, Eperon G E, Ziffer M E, Snaith H J and Ginger D S 2015 *Science* **348** 683–6
[151] Wright A D, Milot R L, Eperon G E, Snaith H J, Johnston M B and Herz L M 2017 *Adv. Funct. Mater.* **27** 1700860
[152] Wang Q, Mosconi E, Wolff C, Li J, Neher D, De Angelis F, Suranna G P, Grisorio R and Abate A 2019 *Adv. Energy Mater.* **9** 1900990
[153] Baloch A A, Alharbi F H, Grancini G, Hossain M I, Nazeeruddin M K and Tabet N 2018 *J. Phys. Chem.* C **122** 26805–15
[154] van der Pauw L J 1958 *Philips Res. Rep.* **13** 1–9
[155] Eliáš P, Hasenöhrl S, Fedor J and Cambel V 2002 *Sens. Actuators* A **101** 150–5
[156] Werner F 2017 *J. Appl. Phys.* **122** 135306
[157] Jerhot J and Šnejdar V 1978 *Thin Solid Films* **52** 379–95
[158] Lindemuth J and Mizuta S-I 2011 *Proc. SPIE* **8110** 811001
[159] Gunawan O, Virgus Y and Tai KFai 2015 *Appl. Phys. Lett.* **106** 062407
[160] Lanza M 2017 *Conductive Atomic Force Microscopy: Applications in Nanomaterials* (New York: Wiley)
[161] Nardi F, Deleruyelle D, Spiga S, Muller C, Bouteille B and Ielmini D 2012 *J. Appl. Phys.* **112** 064310
[162] Frammelsberger W, Benstetter G, Kiely J and Stamp R 2006 *Appl. Surf. Sci.* **252** 2375–88
[163] Lanza M, Porti M, Nafría M, Aymerich X, Whittaker E and Hamilton B 2010 *Rev. Sci. Instrum.* **81** 106110
[164] Tress W, Yavari M, Domanski K, Yadav P, Niesen B, Baena J P C, Hagfeldt A and Graetzel M 2018 *Energy Environ. Sci.* **11** 151–65
[165] Wu W-Q, Rudd P N, Wang Q, Yang Z and Huang J 2020 *Adv. Mater.* **32** 2000995
[166] Tress W 2017 *Adv. Energy Mater.* **7** 1602358
[167] Zhang W, Li Y, Liu X, Tang D, Li X and Yuan X 2020 *Chem. Eng. J.* **379** 122298
[168] Yang Z *et al* 2019 *Nat. Commun.* **10** 1–9

[169] Xie L et al 2019 J. Mater. Chem. A 7 18626–33
[170] Jung E H, Jeon N J, Park E Y, Moon C S, Shin T J, Yang T-Y, Noh J H and Seo J 2019 Nature 567 511–15
[171] Zhang W, Zhang D, Chen Q, Wu J, Ouyang Z and Xia Y 2019 Nat. Commun. 10 79
[172] Huang C, Lin P, Fu N, Liu C, Xu B, Sun K, Wang D, Zeng X and Ke S 2019 Chem. Commun. 55 2777–80
[173] Zhao B, Yan X, Zhang T, Ma X, Liu C, Liu H, Yan K, Chen Y and Li X 2020 ACS Appl. Mater. Interfaces 12 9300–6
[174] Lv Y, Cai B, Ma Q, Wang Z, Liu J J and Zhang W-H 2018 RSC Adv. 8 20982–9
[175] Yang W et al 2020 Nano Energy 67 104189
[176] Zonno I, Martinez-Otero A, Hebig J-C and Kirchartz T 2017 Phys. Rev. Appl. 7 034018
[177] Li Z, Mercado C C, Yang M, Palay E and Zhu K 2017 Chem. Commun. 53 2467–70
[178] Almora O, Zarazua I, Mas-Marza E, Mora-Sero I, Bisquert J and Garcia-Belmonte G 2015 J. Phys. Chem. Lett. 6 1645–52
[179] Almora O, Aranda C, Mas-Marzá E and Garcia-Belmonte G 2016 Appl. Phys. Lett. 109 173903
[180] Von Hauff E 2019 J. Phys. Chem. C 123 11329–46
[181] Fabregat-Santiago F, Garcia-Belmonte G, Mora-Sero I and Bisquert J 2011 Phys. Chem. Chem. Phys. 13 9083–118
[182] Almora O, Cho K T, Aghazada S, Zimmermann I, Matt G J, Brabec C J, Nazeeruddin M K and Garcia-Belmonte G 2018 Nano Energy 48 63–72
[183] Yoo S-M, Yoon S J, Anta J A, Lee H J, Boix P P and Mora-Seró I 2019 Joule 3 2535–49
[184] Wei Z, Chen H, Yan K and Yang S 2014 Angew. Chem. Int. Ed. 53 13239–43
[185] Bisquert J 2003 Phys. Chem. Chem. Phys. 5 5360–4
[186] Guerrero A, Garcia-Belmonte G, Mora-Sero I, Bisquert J, Kang Y S, Jacobsson T J, Correa-Baena J-P and Hagfeldt A 2016 J. Phys. Chem. C 120 8023–32
[187] Contreras-Bernal L, Ramos-Terron S, Riquelme A, Boix P P, Idigoras J, Mora-Sero I and Anta J A 2019 J. Mater. Chem. A 7 12191–200
[188] Miyano K, Yanagida M and Shirai Y 2020 Adv. Energy Mater. 10 1903097
[189] Ng A et al 2018 Adv. Mater. 30 1804402
[190] Wang Z S, Ebadi F, Carlsen B, Choy W C H and Tress W 2020 Small Methods 4 2000290